Manipulation of particles in a Hele-Shaw cell using sources and sinks

Antaran Kumar Deka

Technische Universiteit Delft

Manipulation of particles in a Hele-Shaw cell using sources and sinks

by

Antaran Kumar Deka

in partial fulfillment of the requirements for the degree of

Master of Science
in Mechanical Engineering

at the Delft University of Technology,
to be defended on 01/02/2018.

P & E Report Number : 2879

Supervisor:	Prof. Dr. ir. Jerry Westerweel	TU Delft
Daily Supervisor:	Dr. Daniel Tam	TU Delft
	ir. Ankur Kislaya	TU Delft
Thesis committee:	Dr. ir. Ferdinand Schrijer,	TU Delft
	Dr. Burak Eral,	TU Delft

TU Delft Delft University of Technology

Acknowledgement

I would like to thank ***Dr. Jerry Westerweel*** and ***Dr. Daniel Tam*** for giving me an opportunity to work on this thesis. I would like to acknowledge the guidance and support that I received throughout my work. A very special thanks to ***Ankur Kislaya*** for his supervision and help throughout the entire thesis. Thank you once again for assisting me to plan my schedules and keeping me on track in my work.

I am deeply grateful to ***Jasper Ruijgrok***,for fabricating my experimental set up. I really enjoyed and learnt a lot from the discussions we had. Thank you once again for your expert opinions which helped me in designing my set-up.

A very special thanks to my friend ***Sai Krishna*** for his help, support and suggestions during my entire thesis. Also to ***Aditya Kumar*** for letting me irritate him and making my time more enjoyable.

Last but not the least and most importantly, I am grateful to ***Ma*** and ***Deuta*** for their love, support and patience.

Abstract

The interest in manipulating particles, droplets and bubbles have garnered significant attention in recent years, owing to the advantages offered by micro-fluidics and the advancement in micro-fabrication technologies. These manipulation activities have found its applications in myriad fields of engineering, ranging from medical diagnostics to chemical industry to drug discovery. This has increased demand for the development of devices such as 'Lab on a chip', which performs laboratory-sized experiments and analysis on a single small chip, with the same speed and accuracy as its room-sized counterpart. However, manipulation activities carried out in these devices has fixed channels, designed to serve purpose for specific manipulation tasks. This makes the device suitable for a specific application. Addressing this aspect, a device designed without having any real channels would give an opportunity to integrate multiple functionalities onto a single-chip in the long run. As a first step towards reaching this 'bigger picture', it is necessary to explore the feasibility of manipulating particles, droplets and bubbles by generating so called 'virtual channels'.

The present thesis focuses on an attempt to manipulate particles without the use of any real channels or external field. Although such manipulation is desired in the micro-scale, a top down approach is preferred and hence, the manipulation is carried out in a scaled up model. First, a Hele-Shaw flow cell is designed with sources and sinks in the millimeter scale to deviate streamlines in the same range. Thereafter, four different velocity fields are studied under different combination of sources and sinks, which are then compared to the computational ones. The property of a Hele-Shaw cell that the averaged velocity over the height of the channel is irrotational, makes it possible to compute velocity fields by the use of potential flow theory. The same velocity fields are hence, computed using a discrete source based Panel Method. A good agreement is found between computation and experiment, making PIV measurements not a necessary option for evaluation of velocity fields under these sources and sinks. Finally, individual particle is inserted into the Hele-Shaw cell and manipulated using unsteady fields. The manipulation includes tasks such as diverting particles having same initial position to different end locations; trapping particle for different instances of time and then releasing them into different directions; flipping positions of two particles; and deflecting a particle by ninety degrees. The individual particle trajectory for the above manipulation activities are tracked down using a particle tracking code and then compared with the ones generated using the Panel Method. This, however, excludes the activities where particles need to be trapped because of particle fluctuation near stagnation point. Overall, the Panel Method serves well in predicting particle path-lines and can be used as a tool for manipulating particles.

Contents

Acknowledgement ii

Abstract iii

List of Figures xi

List of Tables xiii

1 Motivation 1
1.1 Outline of the Report . . . 2

2 State of the art Particle Manipulation in Micro-fluidics 3
2.1 Microfluidic physics . . . 3
2.2 Particle manipulation methods . . . 3
2.2.1 Active Manipulation . . . 4
2.2.2 Passive Manipulation . . . 4
2.3 Droplet manipulation . . . 5
2.3.1 Passive techniques . . . 5
2.3.2 Active techniques . . . 6
2.4 Approach . . . 7
2.5 Research Objective . . . 7

3 Design of the flow cell and Experimental set-up 9
3.1 Introduction . . . 9
3.2 Design and fabrication of the flow cell . . . 9
3.2.1 Hele-Shaw cell . . . 9
3.2.2 Flow around a Rankine body and cylinder . . . 10
3.2.3 General consideration and design constraints . . . 11
3.2.4 Designing and dimensioning the flow cell . . . 12
3.2.5 Fabrication . . . 12
3.3 Experimental set up and methods . . . 14
3.4 Design Validation . . . 16
3.4.1 Superimposing uniform flow with a source . . . 17
3.4.2 Superimposing uniform velocity with a dipole . . . 17
3.5 Strength distribution of sources for delivering uniform flow . . . 19

4 PIV study of steady flow fields 21
4.1 Diverting fluid streams . . . 21
4.1.1 Fluid diversion using sources and sinks . . . 22

5 Particle manipulation under unsteady fields **27**
5.1 Flow cell, Particle suspension and particle tracking 27
5.1.1 Flow cell for manipulating individual particle 27
5.1.2 Suspending particles in the fluid 29
5.1.3 Image acquisition and Particle tracking 29
5.2 Observation of individual particle behaviour under the influence of Uniform flow 29
5.3 Experimental generation of unsteady flows and particle manipulation . 31
5.3.1 Sorting particle into different outlets 31
5.3.2 Trapping and steering 34
5.3.3 Flipping particle position 45
5.3.4 Diverting particle by ninety degrees 45

6 Conclusions and Recommendations **49**
6.1 Recommendations for further research 50

A Images **57**
A.1 Particle diversion under unsteady field using a source 57
A.2 Particle diversion under unsteady field using a source and a sink 58
A.3 Trapping and steering straight 58
A.4 Trapping and steering right 59
A.5 Trapping and steering left 59
A.6 flipping particle position 60
A.7 Diversion of particle by ninety degree 60

B Mass flow rate per unit depth **63**

C Panel Method **65**

D Hele-Shaw flow cell equations **67**

List of Figures

3.1 Schematic of a Hele-Shaw cell 10
3.2 Uniform flow superimposed over a flow created by a source. 11
3.3 Uniform flow superimposed over a flow created by a dipole. 11
3.4 The Hele-shaw flow cell, where three filled blue circles at the top representing the upstream sources that drive the uniform flow. The red rectangle represents the 'area of interest'. The red filled circles are downstream sources/sinks used to deflect uniform streamlines. The blue filled circle on this area was used for the initial design. 13
3.5 The Hele-Shaw cell and its components. 14
3.6 a)The Aluminium spacers used to separate the plates b)The plexi-glass plates c)Syringe pumps used to deliver fluid into the set-up d)The clips used to supress the plates. 14
3.7 The connectors fitted to the holes drilled on the plate. 15
3.8 The experimental flow cell and PIV set-up. 15
3.9 Plot of the Maximum Rankine body Height and the free-stream Uniform Velocity at three different flow rates of 50, 70 and 90 ml/hr 17
3.10 Flow around a Rankine body. The red line has twice the length of the maximum height of the Rankine body. 18
3.11 Plot showing the relation between ϵ(distance between the source and the sink)and the radius of the circle. 18
3.12 Flow around an oval body. The red line shows the 'diametric' span of the oval body 19

4.1 Numbering used for sources/sinks. The direction of the free upstream uniform velocity is from left to right. 22
4.2 Flow around "Dual Rankine Body" 22
4.3 Experimental sreamline 23
4.4 Computational streamline 23
4.5 Flow around "Dual Rankine Body" of different widths. 24
4.6 Experimental sreamline 24
4.7 Computational streamline 24
4.8 Flow field in the presence of sources and sinks. 25
4.9 Experimental sreamline 25
4.10 Computational streamline 25
4.11 Flow field in the presence of sources and sinks and devoid of any seeding particle accumulation. 25
4.12 Experimental sreamline 26
4.13 Computational streamline 26

5.1 The modified 2-D top view of the set-up.The green filled circle represents the sources used to deliver the uniform flow. The black filled circle represents the insertion hole for individual particles. The red filled circles represent sources/sinks used to manipulate individual particle. The red area is the region of interest for particle manipulation. 28
5.2 The top-view of the 'area of interest' with the 'sources and sinks' used to manipulate particles. 28
5.3 The y-displacement of particles with respect to time in the 'area of interest' released under the velocity field generated by the upstream sources. The black and light blue lines denote the displacement if particles had moved with the average velocity and maximum centre-line velocity respectively. 30
5.4 The path-lines inside the yellow box skewed at a small angle due to the pinning of the contact angle at the end of the Hele-Shaw flow cell. . . . 30
5.5 Flowrate-time curve of the source used to manipulate the first particle . 31
5.6 Flowrate-time curve of the source used to manipulate the second particle 31
5.7 Pathlines of the two particles diverted into different outlets. 32
5.8 Computational and Experimental Displacement versus Time of the first particle manipulated using a single source. 32
5.9 Computational and Experimental Displacement versus Time of the second particle manipulated using a source 33
5.10 Flowrate-time curve of the source and sink used to manipulate the first particle 34
5.11 Flowrate-time curve of the source and sink used to manipulate the second particle 34
5.12 Pathlines of the two particles. The magenta filled circle represents the sink and the cyan filled circle represents the source used to divert the particles. 35
5.13 Computational and Experimental Displacement versus Time of the first particle manipulated using a source and a sink. 35
5.14 Computational and Experimental Displacement versus Time of the second particle manipulated using a source and a sink. 36
5.15 Pathlines of the trapped particles 36
5.16 Particle fluctuation during the time the particle is being trapped. This is the magnified area around the stagnation region. 37
5.17 Flow-rate time curves of sources used to trap and steer a particle straight. 37
5.18 Particle is trapped in the area inside the rectangular box where a very low velocity region is created.The direction of the flow is from bottom to top. 38
5.19 Displacement versus time of the particle trapped and steered straight. . 38
5.20 Velocity versus time of the particle which is trapped and steered straight. 39
5.21 Flow-rate time curves of sources used to trap and steer particle left. . . 40
5.22 Particle is trapped in the area inside the rectangular box where a very low velocity region is created.The direction of the flow is from bottom to top. 40
5.23 The velocity field will deflect the particle to the left. 40
5.24 Displacement versus time of the particle trapped and steered left. . . . 41
5.25 Velocity versus time of the particle trapped and steered left. 41

5.26 Flow-rate time curves of sources used to trap and steer particle right. . 42
5.27 Particle trapped inside the area of the rectangular box. 42
5.28 The velocity field will deflect the particle to the right. 42
5.29 Displacement versus time of the particle trapped and steered right. . . 43
5.30 Velocity versus time of the particle trapped and steered right. 43
5.31 Flow-rate time curves of sources used to flip particle position. 44
5.32 Particle positions after 2 seconds. 44
5.33 Particle positions after 7sec seconds. 44
5.34 Particle positions after 18 seconds. 45
5.35 Particle positions after 40 seconds. 45
5.36 Flow-rate time curves of sources used to deflect a particle by ninety degree. 46
5.37 Path-line of the particle deflected by ninety degree. 46
5.38 Velocity field used from 9 to 19 seconds from the particle's entry where source 2 is used as a sink. 47
5.39 Velocity field used from 19 to 25 seconds from the particle's entry where source 2 is switched back to a source. 47

A.1 First Particle positions at different instances of time. 57
A.2 Second Particle positions at different instances of time. 57
A.3 First Particle positions at different instances of time. 58
A.4 Second Particle positions at different instances of time. 58
A.5 Images of the particle getting trapped and then being released straight. 59
A.6 Images of the particle getting trapped and then being released right. . . 59
A.7 Images of the particle getting trapped and then being released left. . . 60
A.8 Images of flipping two particles. 60
A.9 Images of the particle deflected by ninety degree. 61

B.1 PIV measurements of the uniform flow 63

C.1 The computational domain of the flow cell with source and collocation points. The three green filled circles represent upstream sources used to drive the uniform flow. The red circle represents the source points whereas the blue circle represents the collocation points. 65

List of Tables

4.1 Image Acquisition details 21

Chapter 1

Motivation

In recent years, manipulation of particles, droplets and bubbles in micro-fluidic devices have been widely investigated and developed, owing to their applications in several fields of engineering, ranging from medical diagnostics to chemical industry to drug discovery. Advances in micro-fabrication technologies have catalyzed the pace of research in the realm of micro-fluidics. The manipulation of bio-particles have become ubiquitous in the field of biological and bio-medical analysis. The different applications within the biological domain where particle manipulation is at the core include particle synthesis[1][2], bio-synthesis[3], cell-biophysics[4][5], cell-drug response[6][7], cell-cell interaction[8][9], single-cell analysis[10] and circulating tumor cell isolation and analyses[11][12] in blood. All of these areas include fundamental operations such as particle separation, focussing, filtering, concentration, trapping, detecting, sorting etc. For these operations to be facilitated, the major task involved is the manipulation of particles. Several new techniques have been deployed and extensive research has been done in order to carry out the aforementioned manipulation tasks. Besides particles, droplet manipulation has also garnered significant attention because of the ability of micro-droplets to ship fluid volume samples through lanes of micro-fluidic networks. Owing to the small scale dimension of a micro-device, it allows small sample volumes, rendering cost-effective and low-risk analysis in drug-discovery, bio-technology and chemical analysis. In oil and gas industry, research have been carried out to predict stability of emulsions through droplet coalescence[13], characterize content of crude oil samples[14], measuring equilibrium gas-oil ratio[15], studying interfacial properties of crude-oil brine[16] any many more. In all of these cases, the underlying principle involved is the manipulation of droplets(production, transport, interaction with other droplets etc.). To this end, the precise manipulation of small particles and droplets has opened new avenues into viewing biological and physical processes with unprecedented levels of control. Recently, there has also been great interest in the manipulation of particle components in the field of self-assembly [17][18][19] for the fabrication of micro-scale and nano-scale devices. The manipulation techniques used for the above tasks are divided into two categories, namely, active and passive. The passive method utilizes the flow field, aided by the channel geometry to manipulate the particle/droplet motion, whereas the active counterpart uses the aid of external fields in order to control their trajectory. Although the existing available techniques show promising performance, they are either too costly in terms of materials or equipments or quite complex. Also, the devices designed for these purposes have fixed channels,

the walls of these channels are micro-fabricated and the channels serve the purpose for only one particular application. Addressing this aspect, if a chip can be designed where no real channels exist, but 'virtual', flexible and multi-purpose channels can be generated, it could potentially integrate the operations mentioned above into one single chip. From performing bio-particle manipulation to characterizing properties of oil, performing multiple chemical reactions/analysis at the same to fabricating micro-machine components, would all be possible on a single platform. Although these are the benefits that could be garnered in the long run, it is first important to check whether generating 'virtual channels' and manipulation of particles/droplets/bubbles is at all possible without having real channels. The current thesis work is dedicated to explore the possibility of particle manipulation without the use of any real channel, but by conforming to the idea of generating 'virtual channels'. A 'top-down' approach is anticipated for this purpose, meaning the manipulation is first intended to be carried out in a scaled-up device before reaching the micro-level.

1.1 Outline of the Report

The report has the following outline. Chapter 2 includes a brief-review of existing manipulation tasks and techniques. The methods used to design the flow cell and the experimental set-up are elucidated in chapter 3. Chapter 4 includes PIV study of steady experimental flow fields and its comparison with computational ones. Particle Manipulation tasks using unsteady flow fields generated by sources and sinks have been described in chapter 5, followed by general conclusions and recommendations in final chapter 6.

Chapter 2

State of the art Particle Manipulation in Micro-fluidics

Micro-fluidic systems have played a major role in performing chemical, biological and analytical analyses in small scales. Along with the advancement in micro-fabrication technologies, the role of micro-fluidics in technologies such as 'Lab-on-a-chip' has become indispensable. In short, 'Lab on a chip' refers to technologies that perform laboratory synthesis and chemical analysis in smaller scales and in a portable device. In addition to this, in-situ analysis and detection of samples are also some of the major tasks that these devices could perform and as fast and accurately as its room-sized counterpart. These devices utilizes the benefits offered by micro-fluidics, with its area of application ranging from life sciences, defense industry, atmospheric science to pharmaceutical science.

2.1 Microfluidic physics

The field of micro-fluidics deals with the movement of fluids in channels with typical dimensions ranging from tens to hundreds of micro-metres. In addition to this, the dynamics of the flow field associated with such magnitude of length scales aids in the effective manipulation of particles and droplets as desired. The important characteristics of flow inside a micro-device includes : negligible inertial and gravitational effects which results in a laminar flow, significant contributions from surface related forces owing to large surface to volume ratio and most importantly diffusion being the most important transport phenomena.

2.2 Particle manipulation methods

Micro-fluidic based particle and droplet manipulation techniques can be broadly divided into mainly active and passive techniques. In the majority of the applications where particle and droplet manipulation is carried out, some of the important particle manipulation tasks involves focusing, separating, trapping and isolating particles,

whereas droplet manipulation tasks involves droplet production, fusion, fission and mixing. Similar principles are used in order to perform these manipulation tasks for both particle and droplets. In the active technique of manipulation, the property of the entity(particle or droplet) is exploited to execute the manipulation, whereas in the passive technique it is the geometry and topology of the micro-channel that is used to manipulate them.

2.2.1 Active Manipulation

In the active manipulation technique, the manipulation is carried out based on the forces exerted by the external interface. The forces used are:

a) **Magnetic :**The magnetic manipulation technique uses external magnetic field, due to which a magnetic force is imposed onto the particle and can be steered accordingly. Applications such as CTC capture[20] and isolation[21], removal of malaria infected RBC's have been reported using this technique.

b) **Electrical :**The electric field technique, commonly called dielectrophoresis incorporates a non-uniform electric field to affect the particles based on the medium and particles' electric properties. Hu et al.[22] performed cell sorting by labelling them with polymeric beads. Concentrating and sorting of cells [23] have also been performed using dielectrophoresis.

c) **Optical:** Radiation pressure of light has also been used to displace and trap micron-sized dielectric particles. This phenomena commonly termed as optical tweezers has been used for single cell, molecule manipulation[24] and also sorting[25].

d) **Acoustics:** The use of ultrasonic standing waves for bio-particle manipulation relies on the creation of ultrasonic standing waves within the channel.A particle in a standing wave field experiences a radiation force which is dependent on the pressure amplitude, volume of the particle and the wavelength. Acoustophoresis has been used in applications such as concentrating bacteria[26] and size based cell separation [27].

2.2.2 Passive Manipulation

Passive methods for particle manipulation relies on hydrodynamic based manipulation. In sch methods, the manipulation is performed by the drag force generated on the particle through specially designed channel geometries and topologies. The different passive methods used in practice are:

a) **Deterministic Lateral Displacement:** Particles are steered into different streamlines by the introduction of pillars and other obstacles. This technique has been deployed in opertions such as isolating cancer cells[28] and separating parasites from blood[29].

b) **Pinched Flow Fractionation:** Introducing contraction/expansion (pinch segment) within the microchannel and in conjugation with the laminar flow profile, particles can also be manipulated to flow at different streamlines,which is known as pinch-

flow fractionation. This technique exploits the property of a particle to follow streamlines passing through its centre-of-mass. This technique has been used for continuous particle separation[30] and focusing[31].

c) **Inertial micro-fluidics:** When in a micro-channel or pipe, the Reynolds number reaches unity and beyond, the inertial effect becomes significant and particle undergoes two types of inertial lift forces. One lift force comes from the shear gradient(acts towards the wall) of the parabolic profile and the other originates from the wall-induced lift(acts away from the wall). The particle comes to an equilibrium position due to the interaction of these two forces. This phenomena is used for particle separation[32], focusing[33], sorting[34] and isolation.

2.3 Droplet manipulation

Similar to particle manipulation, droplet manipulation plays an important role in conducting numerous chemical and biological assays. This is due to the fact fact that when different droplets merge, it facilitates very fast and efficient chemical and biological chemical reactions. This has a distinct advantage over conventional micro-fluidic system for chemical reaction, which suffers from the limited consumption of samples and reagents, less efficient mixing of the samples(mixing only limited to diffusion) and occurrence of dilution and cross contamination of samples resulting from dispersion. Primary operations for droplet manipulation includes droplet formation, droplet fission, fusion , mixing and sorting with applications in the field of single cell analysis, chemical reactions, controlled drug delivery, lab-on-a chip applications and oil-and-gas industry. Similar to particle manipulation, droplet manipulation tasks are accomplished by active and passive techniques.

2.3.1 Passive techniques

Using the channel geometry various droplet manipulation tasks can be performed. Just as the flow velocity inside a micro-channel is directly proportional to the pressure difference and inversely proportional to the hydraulic resistance, the pressure drop across interfaces of droplets can be used to steer droplets. This pressure drop can be directed by confinements created in the micro-channels. This confinement induced interactions can be used to manipulate droplets[35][36]. Using channel geometry technique droplets can be brought into contact with each other, by narrowing the channel, thereby increasing the fluid resistance, which stops the leading droplet and allows the trailing droplet to catch up [37]. Droplets can also be stopped and trapped by an enlargement in the channel [38].Coalescence of droplets can be done even at T-junctions of a channel geometry [39]. Slowing down of droplets, in order to facilitate droplet coalescence, rather than completely trapping them can be done by widening the channel geometry significantly larger than the droplet diameter[40][41]. Using T-junctions[35][42] and Y-junctions[43][44], droplets can also be used for fission.

In another technique, lowered structures('rail system') are embedded in the microchannel to trap droplets. These droplets remain trapped to these structures by lowering their interfacial energy[45].

Droplets are also sorted by utilizing the hydrodynamic flow profile . The important feature which this technique utilizes is that, droplets very small compared to the channel height tends to have a higher velocity than the average mean flow of the continuous phase whereas it is opposite for the larger droplets. Sufficiently small droplets traveling close to the center of the flow profile,however, move faster than the continuous phase and will be trapped at the side walls of the channel behind the large droplet traveling ahead of the small droplets. Droplet sorting has been done in this way[46]. Droplet fission can also be triggered by symmetric micro-fluidic cross flow, leading to the elongation of droplets and eventually into droplet fission in the fluid flow direction[47].

2.3.2 Active techniques

Dielectrophoresis: The process of dielectrophoresis, which refers to the phenomena that a material with a larger dielectric constant that the surrounding medium is attracted to the direction of increasing electric field, can be used to actuate droplets. It has been used for tasks such as redirecting droplets[48] and merge droplets in a flowing medium [49].

Magnetic fields: Magnetic particles impinged onto droplets is used to steer droplets, with the droplets tending to follow the induced magnetic particles [50]. Droplets can be directed through orifices and can also be merged by the above technique. Similar to dielectrophoresis, using magnetic particles in a liquid carrier that will exhibit higher magnetic permeability than the surrounding medium, the droplets can be steered in an inhomogeneous magnetic field as well[51].

Thermo-capillary effect: It uses the principle that the flow of liquid is directed towards region of larger surface tension. Hence, varying the local temperature results in a perturbation of the interfacial tension which results in a movement of the droplet. Trapping and steering of droplets by local heating with a focused laser has been done [52][53].This technique can also be used to coalesce droplets by trapping the first droplet until the second droplet arrives and merges with the first.

Mechanical valves: Droplets can be sorted by increasing the flow resistance of a channel or by blocking the channel entirely using mechanical valves placed outside the micro-fluidic channel. Positions of all droplets within a micro-channel have been freezed by closing all inlets and outlets [54].Recently, the valves has also been embedded into the device. The valves use a second inflatable channel separated by a deformable lamellae. By varying the pressure in the inflatable chamber, the cross-sectional area of the micro-channel can be increased or decreased. A firsthand manipulation of continuous streams of flow was reported in [55]. The technique has also been deployed to sort droplets at frequencies upto hundred hertz [56].

Acoustic streaming: Droplets has also been manipulated using ultrasonic field[57] or surface acoustic waves[58].

2.4 Approach

In this thesis, manipulation of particles is intended to be carried out with the use of sources and sinks. The general aim is to be able to manipulate particles or droplets in a platform which is devoid of any physical channels, so that the same chip can be operated for multiple 'Lab on a chip' based applications. This concept of manipulation, evolves from the works of Tobias M. Schneider, [59] who, inspired by the need to develop novel methods for assembling complex structures from small particles developed a numerical algorithm for assembling complex structures. Their method stems from the observation that a time dependent velocity field will be able to advect particles along arbitrary paths and to arbitrary locations at a fixed time, allowing them to construct micro-structures of high complexity. Based on their algorithm, they successfully manufactured the entire English alphabet using 7 controlled flow rates in two dimension. The present thesis work has a similar approach, as to be able to generate velocity fields that will lead particle to different pre-defined locations. This is done with the aid of sources and sinks, where velocity fields are designed with the aid of Potential flow theory in order to to manipulate particles.

2.5 Research Objective

The present work has the following objective:

a)Designing and constructing a scaled-up micro-fluidic platform(a Hele-Shaw cell)with sources and sinks for particle manipulation in the millimeter range.

b)Comparing experimental steady velocity fields generated by these sources/sinks with computational ones to check the robustness of the code.

c)Finally, introducing individual particle into the flow domain and perform manipulation tasks using unsteady velocity fields.

Chapter 3

Design of the flow cell and Experimental set-up

3.1 Introduction

In order to manipulate particles, a suitable platform is required. The manipulation is intended to be carried out in a Hele-Shaw cell. In this chapter, general considerations in designing the cell, the fabrication process and the experimental set-up is described. The dimensioning used for the design are validated by considering the flow around a Rankine body and the flow due to a dipole, which is described at the end of the chapter.

3.2 Design and fabrication of the flow cell

Before mentioning the general design consideration, a description of the Hele-Shaw cell and its flow -characteristic is given below.

3.2.1 Hele-Shaw cell

A Hele-Shaw cell represents a channel, in which length scales in the stream-wise and span-wise directions of the flow are large compared to the length in the wall normal direction. Figure 3.1 shows the schematic of a Hele-Shaw cell. If U represents a characteristic velocity scale of the flow, with L and h representing two characteristic length scales, non-dimensionalization of the Navier-Stokes equation will reduce it to the Stokes equation, provided the following two conditions are met:

$$L >> h \tag{3.1}$$

$$Re_L(\frac{h}{L})^2 << 1 \tag{3.2}$$

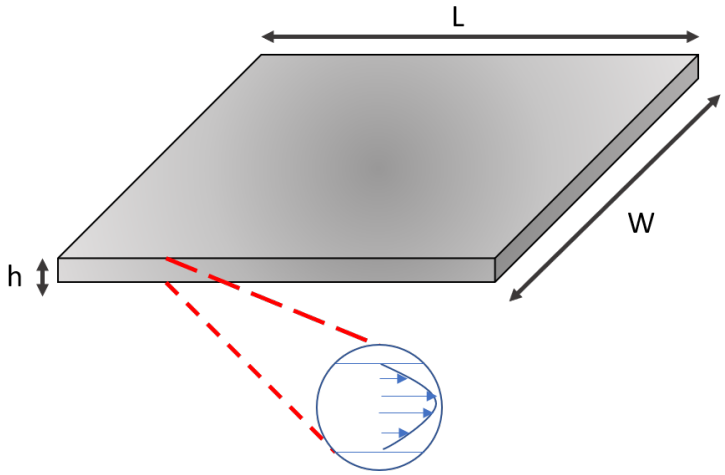

Figure 3.1: Schematic of a Hele-Shaw cell

The final Navier-stokes equation in a Hele-Shaw cell in the absence of body force reads as

$$\frac{\partial u}{\partial x} + \frac{\partial v}{\partial y} + \frac{\partial w}{\partial z} = 0 \tag{3.3}$$

$$\frac{\partial p}{\partial x} = \mu \frac{\partial^2 u}{\partial z^2} \quad \frac{\partial p}{\partial y} = \mu \frac{\partial^2 u}{\partial z^2} \quad \frac{\partial p}{\partial z} = \mu \frac{\partial^2 u}{\partial z^2} \tag{3.4}$$

With w smaller than the horizontal flow speed by a factor of order $O(\frac{h}{L})$, makes pressure a function of x and y alone. This makes integration possible with respect to z for the x and y momentum equation. Integrating and applying no-slip boundary condition at z=0 and z=h, results in a velocity field which is given by

$$u = -\frac{1}{2\mu}\frac{\partial p}{\partial x} z(h - z) \tag{3.5}$$

$$v = -\frac{1}{2\mu}\frac{\partial p}{\partial y} z(h - z) \tag{3.6}$$

The averaged velocity over the height of the cell is obtained by integrating the above two equations over the height of the cell and is read as

$$\mathbf{u} = -\frac{h^2}{12\mu}\nabla P \tag{3.7}$$

As the averaged velocity is the gradient of the pressure field, this means that the velocity field averaged over the height of a Hele-Shaw cell is irrotational. A detailed derivation of the above equations is given in Appendix D.

3.2.2 Flow around a Rankine body and cylinder

Flow around a Rankine body: In potential flow theory, the flow around a Rankine body is produced by superimposing a uniform flow with the flow generated by a source. A source refers to a point of singularity in an incompressible fluid domain where the divergence of the velocity is not equal to zero. It is at this location where a finite

amount of fluid mass is introduced into the domain. A schematic of the flow around a Rankine body depicting its maximum half-width is shown in figure 3.2. The maximum half-width of the Rankine body is given by

$$h_{max} = \frac{m}{2U} \tag{3.8}$$

where **m** is the mass flow rate per unit depth at the location of the source and **U** is the upstream uniform velocity.

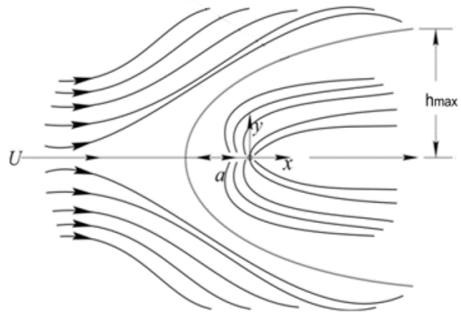

Figure 3.2: Uniform flow superimposed over a flow created by a source.

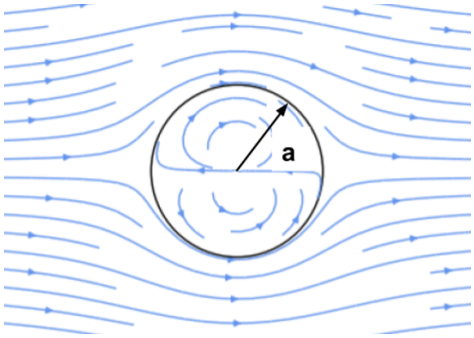

Figure 3.3: Uniform flow superimposed over a flow created by a dipole.

Flow around a cylinder: Similar to the flow around a Rankine body, superimposition of a uniform flow and the flow due to a dipole results in a flow around a cylinder. Dipole refers to a combination of a source and a sink separated by an infinitesimal distance. The direction of the dipole strength is such that it is aligned in a direction opposite to the flow direction. Similar to the concept of source, sink refers to a singular point where a finite amount of fluid mass is consumed from the fluid domain. Schematic of the flow around a cylinder is given in figure 3.3. The strength of the dipole to create a radius of 'a' is given by

$$d = 2\pi a^2 U \tag{3.9}$$

where,

$$d = 2m\epsilon \tag{3.10}$$

which represents the strength of the dipole, m represents the flow rate per unit depth at the location of the source and sink, and ϵ represents the separation distance between the source and sink.

3.2.3 General consideration and design constraints

Following considerations are taken into account in designing the Hele-Shaw flow cell:

a)A scaled up-device is intended from a micro-level. This implies streamline diversion used for manipulation is also expected in the same range. The flow around a Rankine body and the flow around a cylinder is considered for that purpose. The dimension of the maximum half-width of the Rankine body and the radius of the cylinder gives an

estimate of the order of magnitude of the uniform streamline diversion. Hence, it is considered to keep these dimensions in the millimeter range.

b)Hele-Shaw flow conditions as mentioned in eq(3.1) and eq(3.2 has to be satisfied, if particle manipulation is to be carried out with the aid of Potential flow theory.

The design constraints include:

a)The syringe pumps, with a maximum delivering capacity of 99 ml/hr.

b)The syringes with a capacity of 50 ml.

c)The drilling equipments available and their size. Sizes are of order O(1) mm.

d)The type and size of the fittings used to connect pipes to the source/sink.

3.2.4 Designing and dimensioning the flow cell

The Hele-shaw cell is designed with two glass plates mounted on top of one another. An aluminium spacer sandwiched between these two plates serve as the gap(height) of the flow cell, in addition to forming the side walls. It is within this gap where fluid flow takes place. This design allows for the gap between the plates to be varied according to the thickness of the spacers used. The gap thickness used is 1.5 mm, owing to less leakage from the flow cell at this gap spacing. The width of the flow cell is kept at 100 mm, as streamline deflections within the flow cell are intended to be in order of O(10)mm. An order of O(10)mm is chosen for the deflection, owing to the fact that sources/sinks have a diameter of 2 mm. Also, a 100 mm width ensures that side walls of the flow cell does not have significant impact in the 'area of interest'. Three fluid sources on the top plate are intended to drive the flow within the gap of the flow cell. Three fluid sources are chosen considering the fact that an individual syringe has a volumetric capacity of 50 ml, which is not sufficient to maintain the fluid flow for a longer time. The length of the Hele-Shaw cell is kept at 300 mm. Two factors influence the choice of this length. First, the flow from the upstream three sources become parallel only after 30 mm from them. Second, the area where the manipulation task is to be carried out is intended to be at a considerable distance from the end of the flow cell. Initial design of the flow cell consisted of a single downstream source to deflect uniform streamlines, situated at a distance of 165 mm from the 'upstream sources' . The final design consists of four downstream holes(to be used as sources and sinks) in the 'area of interest', arranged in a diamond shaped pattern . These holes are separated by a distance of 16 mm in the horizontal and vertical direction. The dimensions of connectors used to insert pipes into these holes are taken into account while choosing this dimension. A schematic of the final design with its dimension are shown in figure 3.4.

3.2.5 Fabrication

The Hele-Shaw flow cell is constructed with two Plexi-glass plates of length 310 mm and width 120 mm which are mounted on top of the other. Three aluminium spacers of width 10 mm and thickness 1.5 mm are sandwiched between these plates to serve

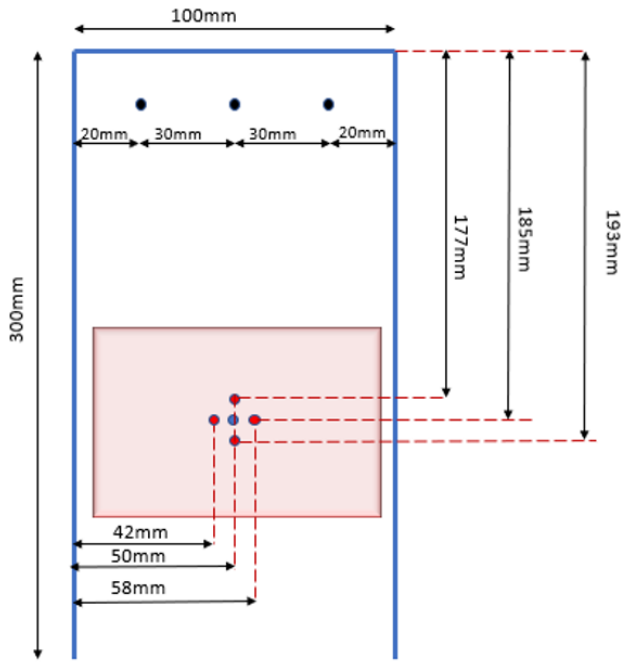

Figure 3.4: The Hele-shaw flow cell, where three filled blue circles at the top representing the upstream sources that drive the uniform flow. The red rectangle represents the 'area of interest'. The red filled circles are downstream sources/sinks used to deflect uniform streamlines. The blue filled circle on this area was used for the initial design.

as walls of the flow cell. These spacers maintain a gap between the Plexi-glass plates, thus, serving as the fluid domain. The spacers are placed in a U-shaped pattern, covering three sides of the Plexi-glass. One end is left open to the atmosphere for the fluid to drain out. Plastic clips are used to suppress the two plates. The clips are placed uniformly along the perimeter of the plates to maintain uniform compression.

Holes of size 2 mm are drilled to act as sources and sinks. Pipes of 4 mm inner diameter are used to deliver fluid in or out of the flow cell. One end of the pipes are inserted into these holes via connectors shown in figure 3.7, while the other end is connected to syringes. The syringe pumps used to deliver the uniform flow can be used only as sources, whereas those used to divert streamlines in the downstream region can be used both as sources and sinks. The connectors (luer)which connects holes to the pipes, consists of a male and a female luer. The male luer is shown on the right of figure 3.7 whereas the female luer on the left. The threaded side of both the luers are fitted to the bottom plate of the Hele-Shaw cell. With respect to the male luer, one end is fitted to the hole whereas the other end is connected to the pipe used for draining fluid in or out of the flow cell. Whereas for the female luer, a check valve is connected to its other end instead of a pipe. This check valve blocks the fluid to drain in or out of the flow cell through the hole to which it is attached. The female luer is used when a source is not in operation either as a source or a sink.

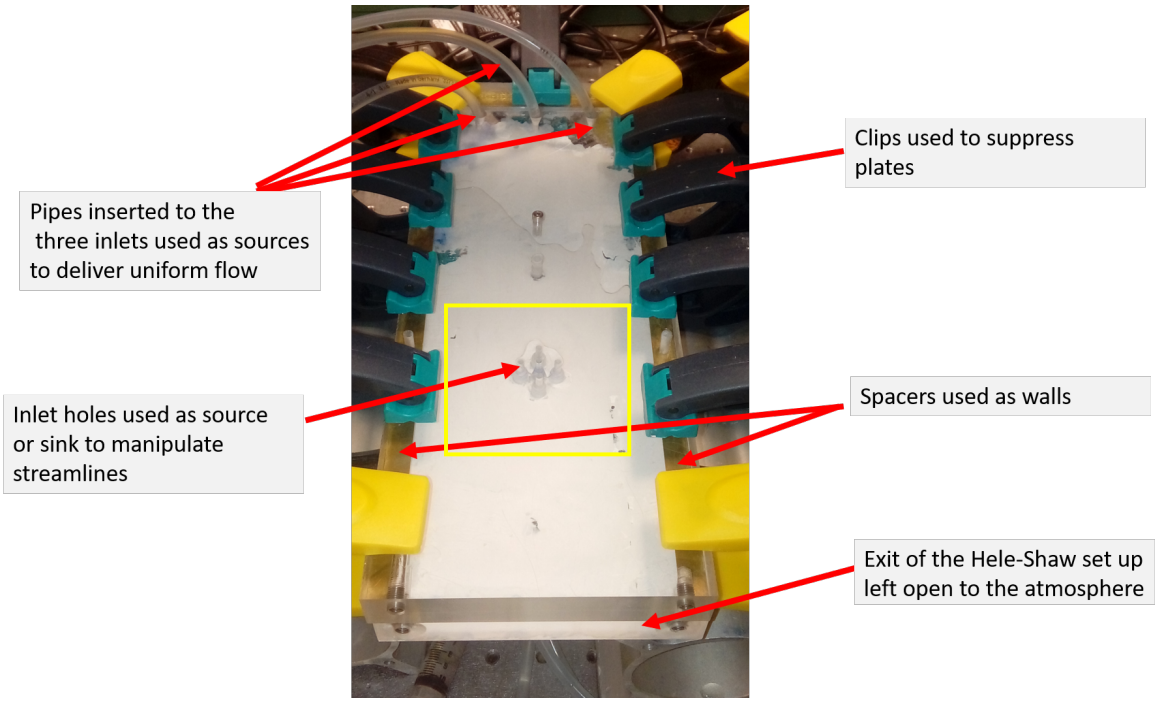

Figure 3.5: The Hele-Shaw cell and its components.

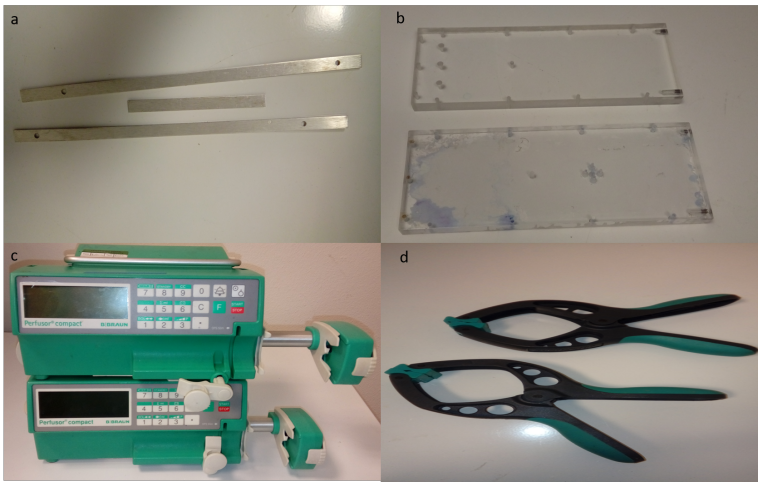

Figure 3.6: a)The Aluminium spacers used to separate the plates b)The plexi-glass plates c)Syringe pumps used to deliver fluid into the set-up d)The clips used to supress the plates.

3.3 Experimental set up and methods

The experimental set-up is shown in figure 3.8. The Hele-Shaw flow cell along with its components is mounted on top of two beams so that it remains perfectly horizontal. The camera is placed directly above the 'field-of-view' or the 'area of interest'. The field-of-view is illuminated by LED light which is also placed above the flow cell. Syringe pumps are placed on the side of the flow cell to deliver the fluid. In the present work, experimental studies of different steady velocity fields are performed, using optical imaging technique called Particle Image Velocimetry. A brief description

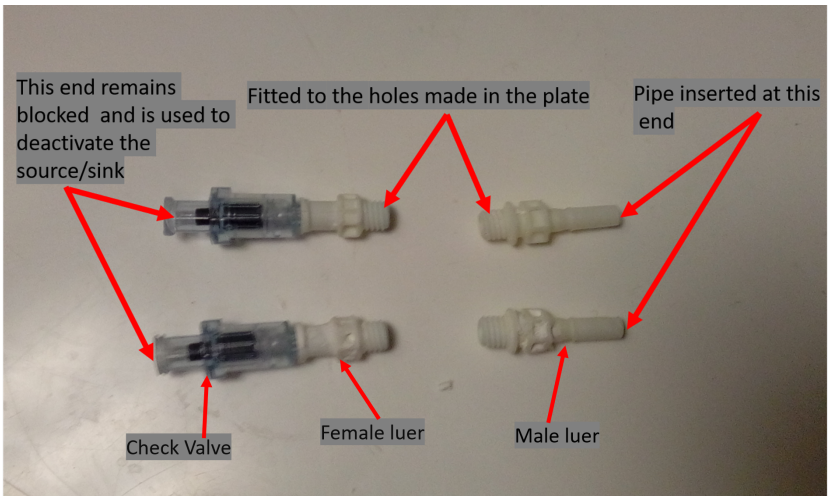

Figure 3.7: The connectors fitted to the holes drilled on the plate.

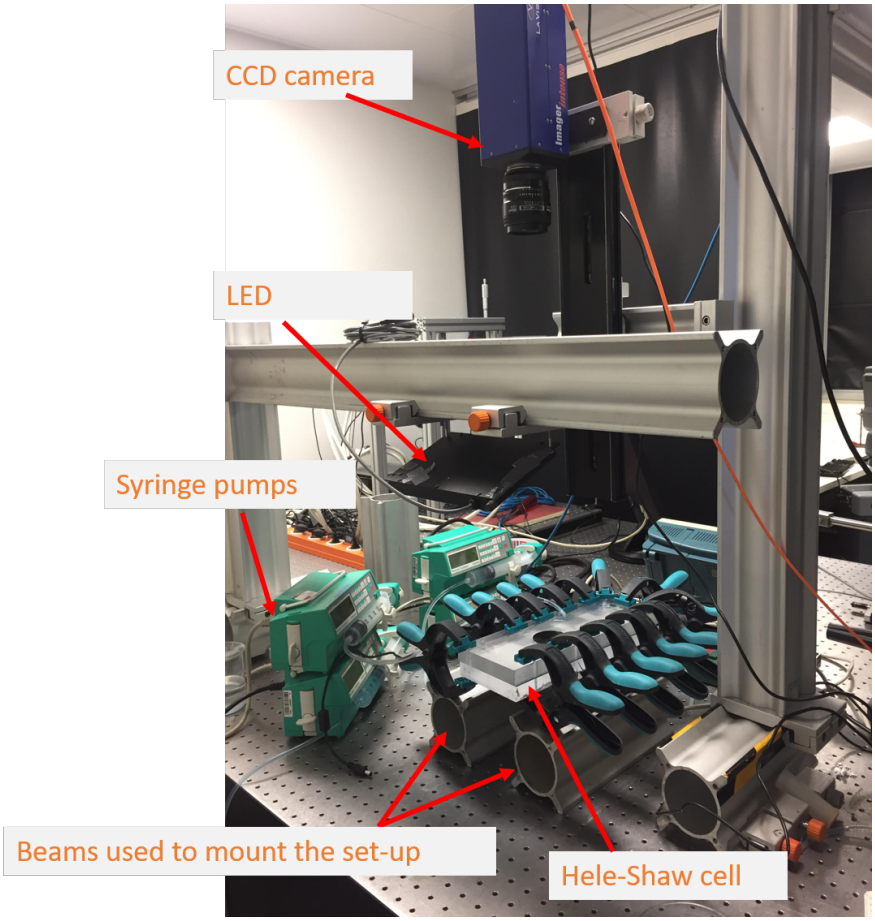

Figure 3.8: The experimental flow cell and PIV set-up.

of the technique is provided in this section.

Particle Image Velocimetry is a non-intrusive flow measurement technique that has been routinely used to procure quantitative information about two-dimensional velocity fields by analyzing the motion of tracer particles suspended in the fluid. It uses a statistical approach to measure the velocity fields. Contrary to the methods where individual particles are tracked, this method evaluates the displacement vectors

by dividing the area of interest into so-called interrogation regions. The intensity field of each of such interrogation region are cross-correlated with the corresponding regions of subsequent images to obtain a cross-correlation function. The location of the peak of the function provides the displacement of the particles and hence, the direction and magnitude of the velocity. For more details on PIV, the following book [60] is to be referred. Conventionally, the illumination of two-dimensional PIV is done by a light sheet whose thickness is less than the depth of field of the image recording system, in which case the depth of the measurement plane is determined by the thickness of the light sheet. Volumetric illumination is an alternative approach where the area of interest is illuminated by a volume of light. Volume illumination is a suitable mode for the present study owing to the fact that optical access is limited to only one direction and the separation between the plates is only 1.5 mm. As far as the correlation technique is concerned, "sum of correlation" is used for the present purpose, considering the fact that seeding density of the particles should be kept low in order to avert clogging of particles and particle jamming at the inlet hole.

Volume illuminated PIV measurements are performed to obtain the experimental streamlines of four different combinations of sources and sinks. The flow is illuminated by LED light, with the images being acquired by a single frame CCD camera (LaVision, Imager Intense). For every PIV measurement, the carrier fluid is seeded with 90-106 micron grey polyethylene micro-sphere tracer particles. The particles have a density of 1.002 g/cc. The particles are well suspended in water before being used for the experiment. Before evaluating the vector fields, background subtraction is performed to remove noise as an image pre-processing step. This is done by first inverting the image, and subsequently applying a time series filter with a background average subtraction. The resulting images are interrogated in a 32X32 pixels window size with a 50 percent window overlap. A sequential cross correlation is used to obtain the vector fields, where one correlation function is obtained from a pair of images and then subsequently added to obtain the final vector frame. As is the case with 'Sum of correlation', the quality of the correlation function is directly proportional to number of images taken, maximum number of images possible were acquired. The number of images possible for all experiments are a result of the frequency of image acquisition and the capacity of the syringe pumps. As the syringe pumps have a capacity of 50 ml, and the frequency of image captured is 2Hz, images in the range of 3000 are possible to be taken. Spurious vectors are removed by applying a median test(universal outlier detection). The image density for the experiments are found to be 3 pixels per 32X32 interrogation window, with a typical particle image diameter obtained as 2 pixels.

3.4 Design Validation

In order to validate the design of the flow cell, two experiments are performed with water as the working fluid, namely, the flow around a Rankine body, generated by a single downstream source and its interaction with the uniform flow. Secondly, the flow around a cylinder, which is generated by a source and sink in the downstream area interacting with the uniform flow.

3.4.1 Superimposing uniform flow with a source

According to equation 3.8, if a maximum half width of Rankine body of order O(10)mm is to be obtained, the uniform free-stream velocity should be of order O(0.1) mm/sec on using a downstream source strength of 70 ml/hr. Figure 3.9 shows the trend. It is important to note that the Hele-Shaw flow condition, on maintaining an average velocity of the above magnitude reads as $Re_L(\frac{h}{L})^2 = 0.0015$, for the dimensions considered in the flow cell design. Streamlines obtained on superimposing a uniform flow

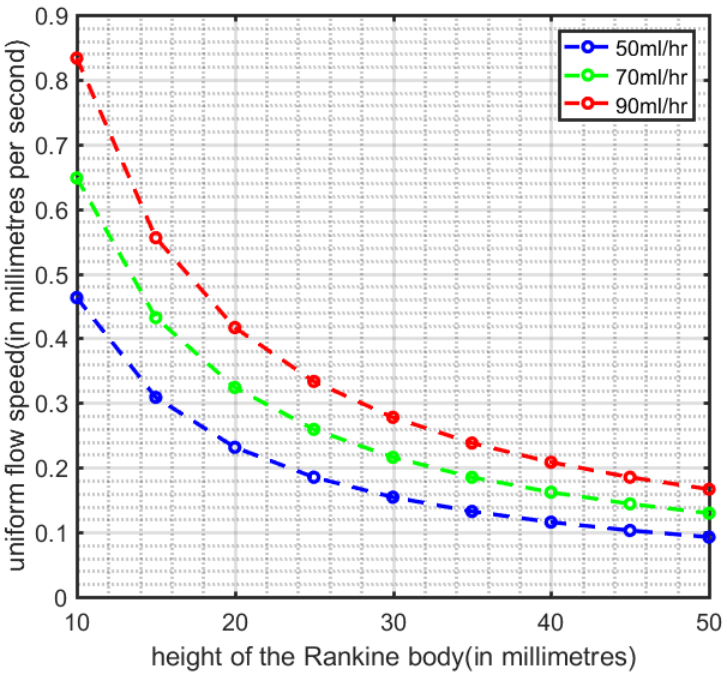

Figure 3.9: Plot of the Maximum Rankine body Height and the free-stream Uniform Velocity at three different flow rates of 50, 70 and 90 ml/hr

of average magnitude 0.2 mm/sec, with a flow generated by a downstream source of strength 70 ml/hr is shown in fig 3.10. It can be clearly seen from the image that dimensions of the maximum half-width fall into the expected range. It is, however, to be mentioned that PIV measurements are not done for this experiment. To get such an image, the flow is seeded with same particles to be used for PIV measurements, with subsequent acquisition of around 2000 images. The minimum background intensity of all images are then subtracted from individual images to acquire the above one.

3.4.2 Superimposing uniform velocity with a dipole

It has been mentioned previously that superimposing a uniform free stream flow with a dipole results in the 'flow around a cylinder'. From equation 3.9 and 3.10, a relation between the diameter of the cylinder, and the separation distance between the source and sink(dipole) of the resulting dipole can be obtained. This relation reads as mϵ=π a^2U. Ideally, to replicate a full circle ϵ tends to zero, which is not possible physically. Maintaining a finite value of ϵ will lead the circle to deviate to an oval body. In the

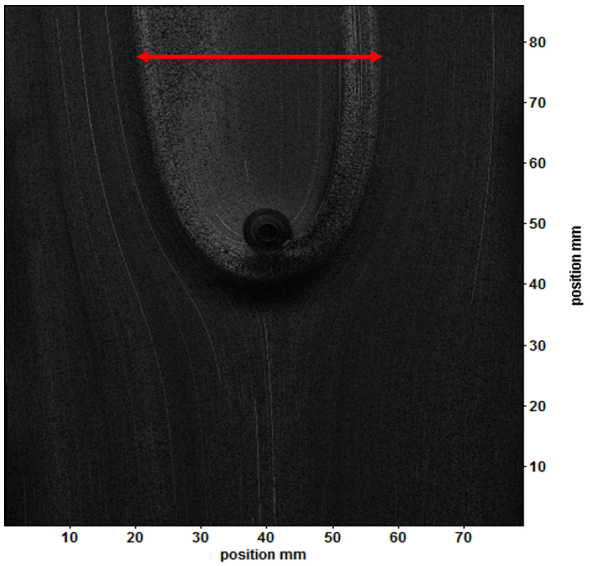

Figure 3.10: Flow around a Rankine body. The red line has twice the length of the maximum height of the Rankine body.

present case, however, we approximate the oval body to be a circle. A plot showing the relationship between the separation distance and the radius of the circle is shown in figure3.11. Three different flow rates of 50,70 and 90 ml/hr are considered, which are normalized by the gap of the flow cell (1.5 mm) to obtain the value of **m**. The free-stream uniform velocity is taken as 0.2 mm/sec. An experiment is performed with

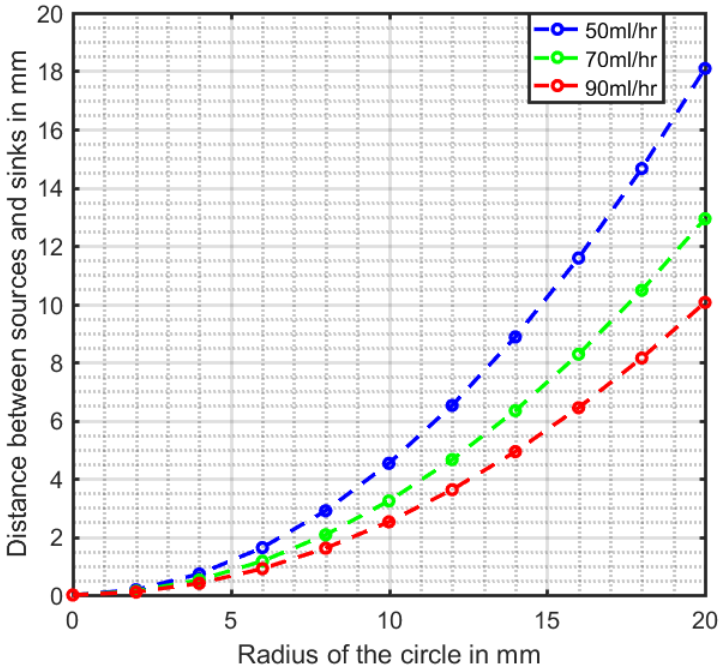

Figure 3.11: Plot showing the relation between ϵ(distance between the source and the sink)and the radius of the circle.

a free stream uniform velocity of around 0.2 mm/sec, and the individual source-sink strengths of the dipole as 70 ml/hr. The separation distance between the source and

the sink is maintained at 8 mm. Figure 3.12 shows the result of the experiment. The diameter of the oval body as highlighted by the red line falls into the expected range when compared with the previous plot.

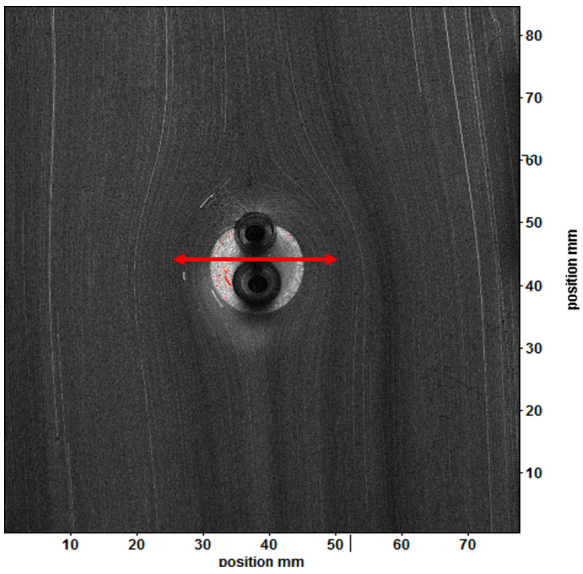

Figure 3.12: Flow around an oval body. The red line shows the 'diametric' span of the oval body

3.5 Strength distribution of sources for delivering uniform flow

In order to find the strength distribution of upstream sources that would procure a uniform velocity magnitude of order O(0.1)mm/sec, a discrete source based Panel Method is used. The results from the Panel method sets a strength distribution of 50 ml/hr for each source near the side walls and 25 ml/hr for the middle source to obtain velocity of the aforementioned magnitude. Also, it is found that uniform parallel streamlines are obtained at approximately 30 mm from these sources. This value, which sets the lower limit, is considered while deciding the length of the flow cell.

Chapter 4

PIV study of steady flow fields

In this chapter, four different steady velocity fields obtained from PIV measurements are shown. The working fluid is water. These velocity fields are a result of the operation of four different source/sink configuration in the 'area of interest'. Velocity fields of the same source/sink configuration are then computed using a discrete source based Panel method. A detailed description of the Panel Method is given in Appendix C. The experimental and corresponding computational velocity fields are then compared, in order to check the robustness of the code. In all of these experiments, the upstream uniform flow is driven by three sources having strengths of 50ml/hr, 25ml/hr and 50ml/hr. As obtained from the Panel code, these three sources yield a uniform free-stream velocity of around 0.2 mm/sec, as long as the gap of the flow cell is maintained at 1.5 mm.

4.1 Diverting fluid streams

The sources/sinks in the area of interest are shown in figure 4.1. Different velocity fields are obtained in the experiment by utilizing these sources distinctly. The numbering of sources/sinks provided in the figure will be used in the remainder of this chapter. The image acquisition details of the four experiments is listed in table 4.1.

Table 4.1: Image Acquisition details

Experiment number	Acquisition Frequency(Hz)	Magnification	Focal Length(mm)	f-stop	Field of view(mmXmm)
1	2	0.133	35	8	78.220 X 85.331
2	2	0.13	35	8	68.018 X 74.202
3	2	0.13	35	8	68.018 X 75.293
4	2	0.13	35	8	68.018 X 75.293

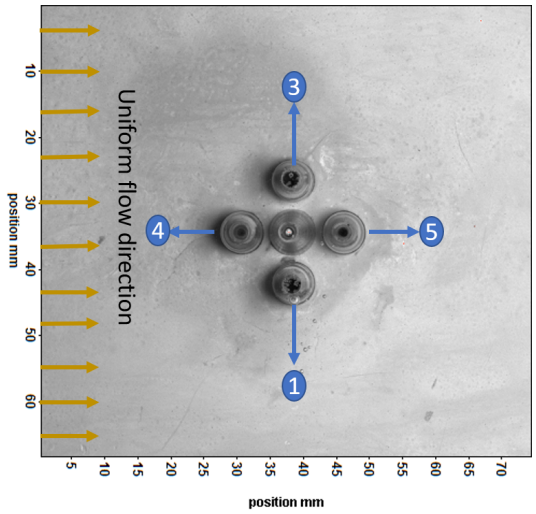

Figure 4.1: Numbering used for sources/sinks. The direction of the free upstream uniform velocity is from left to right.

4.1.1 Fluid diversion using sources and sinks

Two experiments are performed using only sources to procure different steady velocity fields. In these two experiments, configuration of active sources remain the same, only the strength varies.

Experiment 1 produce streamlines of "Dual Rankine body" type, with both downstream sources, denoted by 1 and 3 in figure 4.1 having the same flow rate of 70 ml/hr. The actual image of the velocity field at a given instant after background image subtraction is shown in figure 4.2. Fig 4.4 shows the computational streamlines using the Panel Method, while figure 4.3 shows the experimental one. The deviation comes in

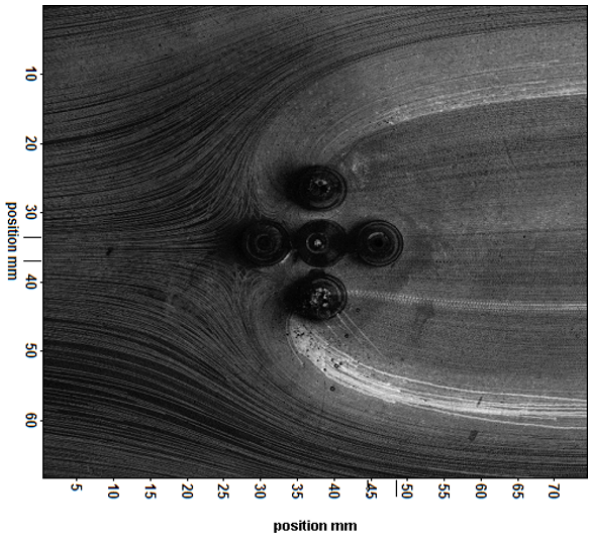

Figure 4.2: Flow around "Dual Rankine Body"

the region where the deactivated source (4) is located. Because of its presence, particles flowing over this source are not properly captured. As a result, velocity vectors deviate from the computed ones in the area surrounding the above source. The second

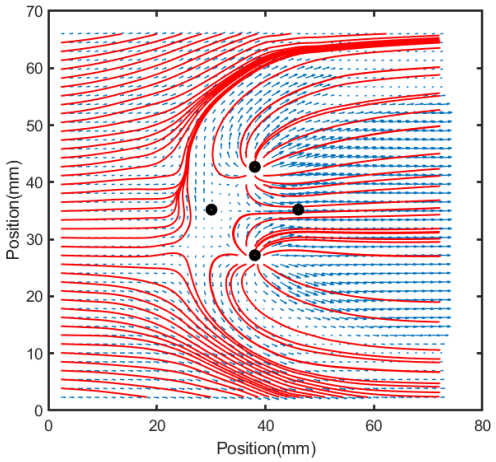

Figure 4.3: Experimental sreamline

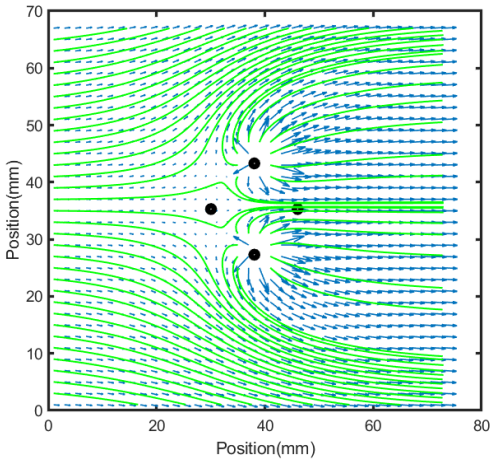

Figure 4.4: Computational streamline

discrepancy occurs in the region surrounding the stagnation point(more precisely very low velocity region, as a clear stagnation point might not be present for the above configuration) in front of sources 1 and 3. This is because PIV particles surpassing this region are not completely held static. Instead, they tend to fluctuate at and around stagnation points, in addition to being constantly bombarded by the incoming upstream flow of particles and particles emanating from the nearest source. When these fluctuating particles, present within the area of very low velocity region are hit by incoming group of particles, they tend to follow different streamlines of the flow. These motion of particles lead to spurious vectors in the area surrounding stagnation point. However, apart from these regions, a reasonable agreement is found between theory and experiment in the rest of the domain.

Experiment 2 includes the same configuration as that in experiment 1, with the strength of the lower source being reduced to half the value of the upper source. As can be seen from figure 4.6 and 4.7, a good match is observed between computation and experiment, with both velocity fields being able to capture the differences in width of the upper and lower Rankine Body. Similar to the previous experiment, there exists a mismatch of streamlines in the region where source 4 is located. This can again be attributed to the presence of the source and stagnation region. Figure 4.5 shows streaks of particles in the velocity field of experiment 2.

Experiments 3 and 4 includes the introduction of sinks in order to divert uniform streamlines. In **experiment 3**, source 1 and 4 operates at 70 ml/hr whereas sink 5 operates at -70 ml/hr. Similar to previous experiments, there exists a mismatch in the area where stagnation region is located. The experimental and computed velocity fields are shown in figures 4.9 and 4.10. Excluding the area near stagnation point, the computed streamlines conform to the experimental one in the rest of the domain. Figure 4.8 shows the raw image of particle sreaks.

In **experiment 4**, source 1 and 3 operates at 70 ml/hr and sink 4 at -70 ml/hr. Although there exists a very small velocity region in front of source 1 and source 3, the particles at this region are constantly under the influence of sink 4, and hence does not accumulate. In the absence of particle accumulation due to the presence of sink 4, it can be seen that the measurement obtained from PIV and computation is in good

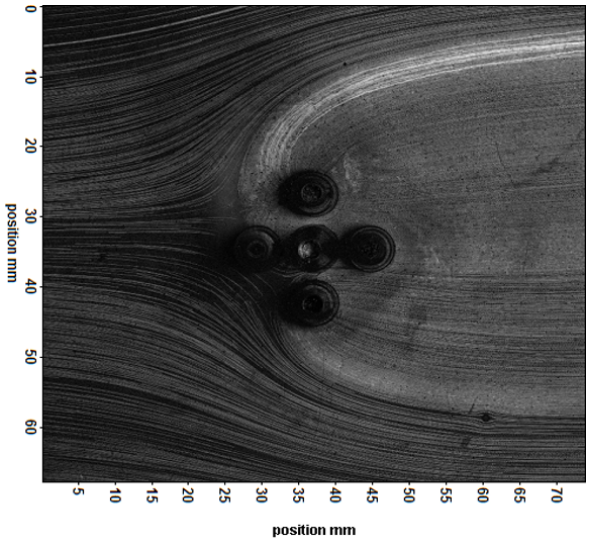

Figure 4.5: Flow around "Dual Rankine Body" of different widths.

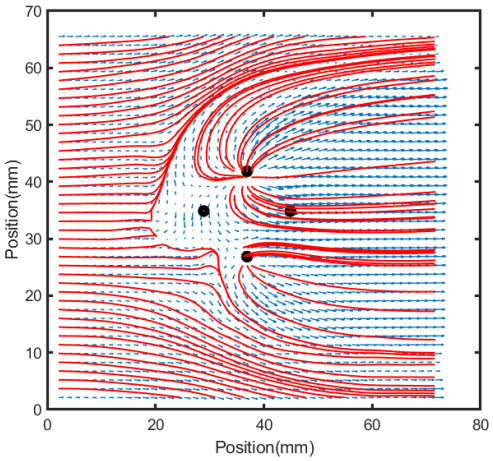

Figure 4.6: Experimental sreamline

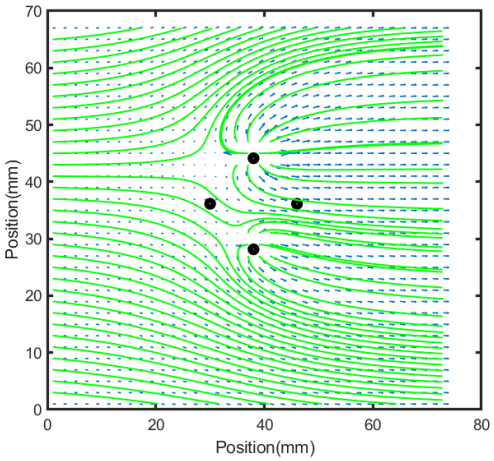

Figure 4.7: Computational streamline

agreement in the entire domain. This experiment serves well to manifest the effect of particle accumulation within stagnation regions into the PIV result. Figure 4.11 shows the streamlines in the actual image. Fig 4.12 and Fig4.13 shows the experimental and computational streamlines derived from PIV measurements and the Panel Method respectively.

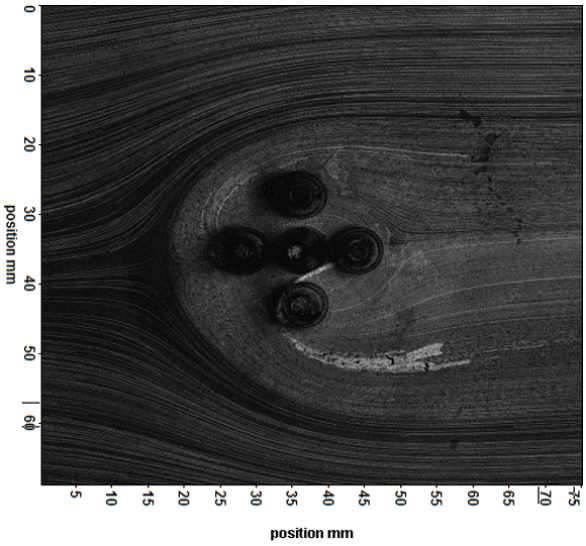

Figure 4.8: Flow field in the presence of sources and sinks.

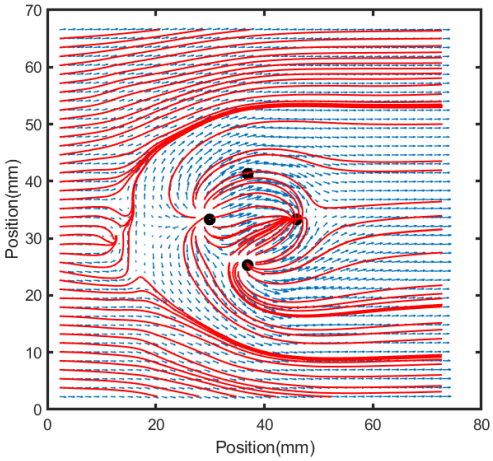

Figure 4.9: Experimental sreamline

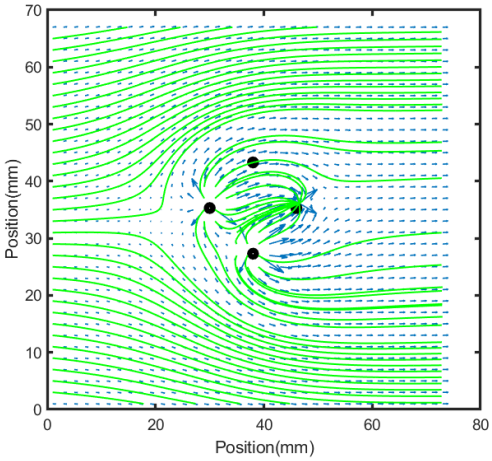

Figure 4.10: Computational streamline

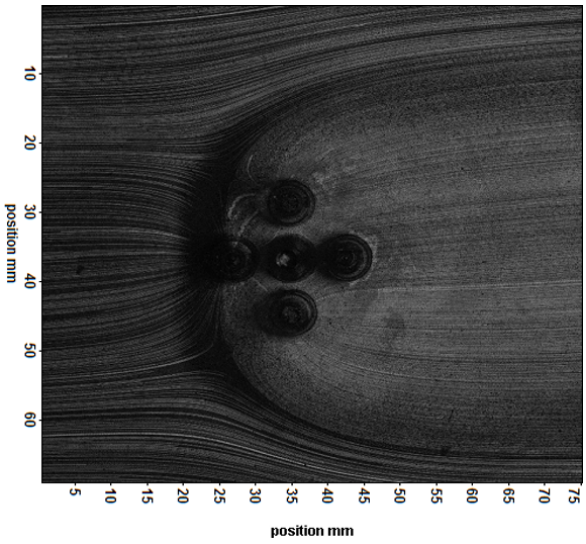

Figure 4.11: Flow field in the presence of sources and sinks and devoid of any seeding particle accumulation.

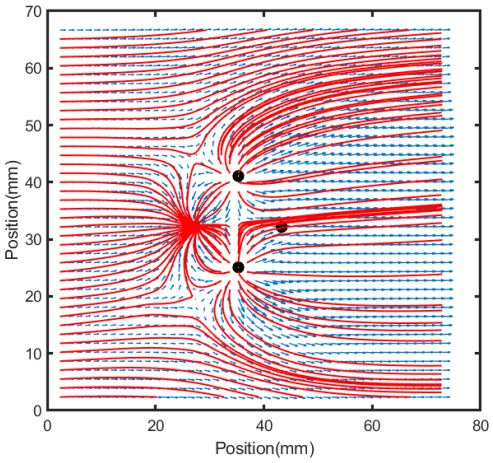

Figure 4.12: Experimental sreamline

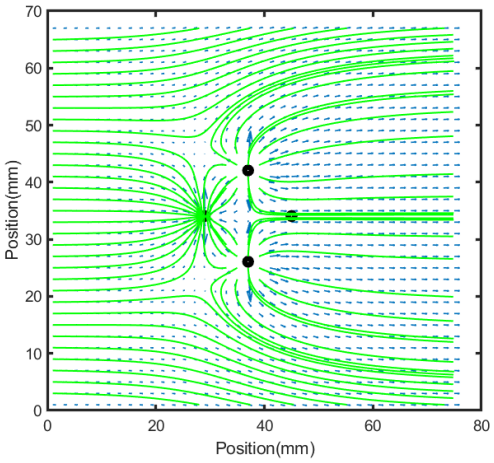

Figure 4.13: Computational streamline

Chapter 5

Particle manipulation under unsteady fields

In this chapter, attempts made to manipulate individual particles have been described. These individual particles have been manipulated using unsteady fields. Particle manipulation tasks involving unsteady velocity fields include diverting individual particle having same initial position to different locations, trapping a single particle and diverting it in different direction, and flipping the position of two particles.

5.1 Flow cell, Particle suspension and particle tracking

5.1.1 Flow cell for manipulating individual particle

In order to manipulate single particle using unsteady fields, an additional hole has been drilled at a distance of 100 mm from three upstream sources generating the uniform flow. This distance is chosen such that particles have sufficient time to adjust itself to the upstream uniform flow as it enters the 'field of view'. Moreover, the flow cell gap is reduced to 0.5 mm, in addition to increasing the total flow rate used to deliver the upstream uniform flow. The strength of each source, following the steady experiments has been increased to twice the magnitude. This is done such that sufficient drag is generated in order to accelerate the particle to attain the velocity of the uniform flow. A schematic of the modified 2-D diagram is shown in figure 5.1. The green filled circles near the side walls have a flow rate of 100 ml/hr and the middle green filled circle has a strength of 50 ml/hr. Also, the actual image of the field-of-view region is shown in figure 5.2, with the numbering of sources/sinks. The sources and sinks would be referred to by these assigned numbers in the rest of the chapter.

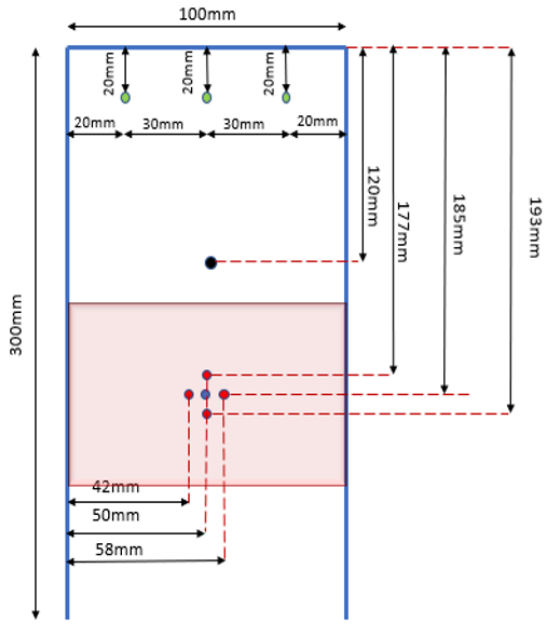

Figure 5.1: The modified 2-D top view of the set-up.The green filled circle represents the sources used to deliver the uniform flow. The black filled circle represents the insertion hole for individual particles. The red filled circles represent sources/sinks used to manipulate individual particle. The red area is the region of interest for particle manipulation.

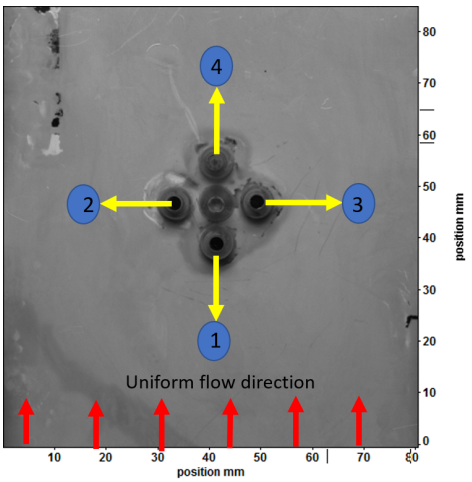

Figure 5.2: The top-view of the 'area of interest' with the 'sources and sinks' used to manipulate particles.

5.1.2 Suspending particles in the fluid

Particles used for manipulation are polyethylene micro-spheres, with diameters ranging from 355 to 425 microns, and having a density of 0.993 g/cc. In order to suspend them into the fluid, the following procedure is followed: A container is filled with the desired amount of de-ionized water and heated until the water reaches a rolling boil. The water is left boiling for approximately 5 minutes. While the water is heating, 0.10 grams of Tween per 100 ml of water is mixed with a magnetic mixer. Once mixed, 0.1 percent Tween solution is prepared. When finished, the solution looks clear and uniform. Once the solution is prepared, using a vial, 0.5 grams of micro-spheres are taken, and 2 ml of the 0.1 percent Tween solution is added. The solution is then centrifuged for 5–10 minutes to get the spheres wetted and into solution.

5.1.3 Image acquisition and Particle tracking

In all experiments, the images of particles have been recorded similar to PIV measurements. The images have been acquired with a frequency of 2 Hz using LaVision Imager Intense camera. A 35 mm lens has been used for recording. Once images are acquired, individual particles have been tracked by developing a particle tracking code in MATLAB. The images acquired are first inverted, and then background subtraction is performed in DAVIS 7.2, before performing further processing to track them. Once an individual particle is tracked in every image, the positions are connected to construct path-lines. The experimental path-lines are then compared with the computed ones using a discrete source based Panel Method.

5.2 Observation of individual particle behaviour under the influence of Uniform flow

Before proceeding with experiments involving individual particle manipulation, it is necessary to check the magnitude of their uniform velocity, or whether particles move with a sufficiently uniform velocity at all. In order to observe the particle behaviour under the uniform flow in the 'area of interest', a series of particles are released and their displacements in the stream-wise direction(y-direction) are noted down. A plot of the measured y-displacement with respect to time is shown in figure 5.3. The measured plot are straight lines with uniform slopes. Hence, almost all particles that are released have a velocity constant in time when driven by upstream sources, except that there is a difference in the measured velocity magnitude. This can be attributed to the different equilibrium positions that particle tend to occupy based on their size. From the above experiment, it is also clear that particles adapt itself to the flow by the time it reaches the field of view. In addition to this, particles released were also seen to have a certain skewness from its straight trajectory. This is because of the pinning of the contact angle at the outlet of the Hele-Shaw cell, which led the fluid to be drained out of the cell from a single point rather than the entire outer edge. This skewness is shown in figure 5.4.

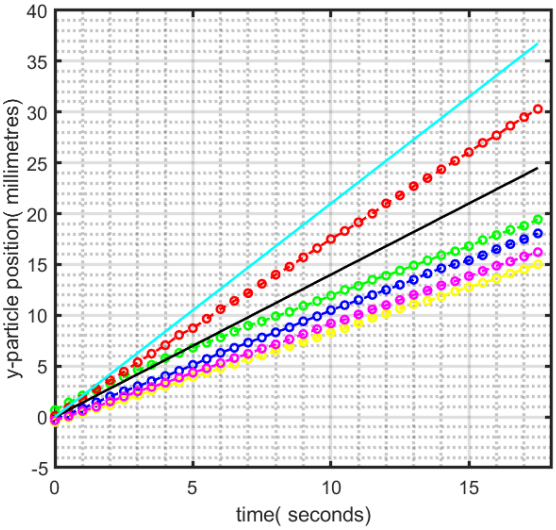

Figure 5.3: The y-displacement of particles with respect to time in the 'area of interest' released under the velocity field generated by the upstream sources. The black and light blue lines denote the displacement if particles had moved with the average velocity and maximum centre-line velocity respectively.

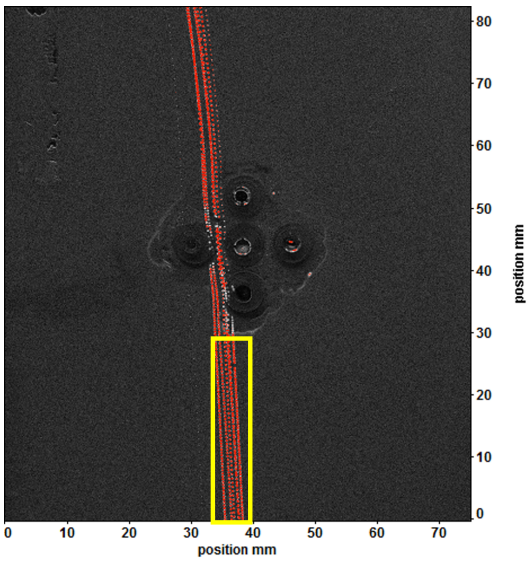

Figure 5.4: The path-lines inside the yellow box skewed at a small angle due to the pinning of the contact angle at the end of the Hele-Shaw flow cell.

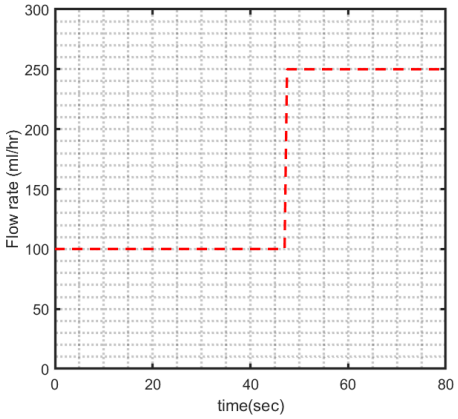

Figure 5.5: Flowrate-time curve of the source used to manipulate the first particle

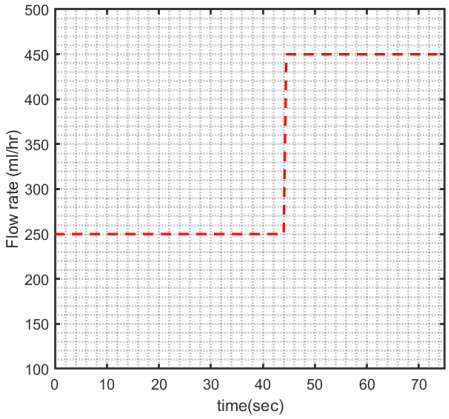

Figure 5.6: Flowrate-time curve of the source used to manipulate the second particle

5.3 Experimental generation of unsteady flows and particle manipulation

5.3.1 Sorting particle into different outlets

In the following experiments, two separate individual particles are diverted into different outlets by using unsteady fields. In the first experiment, only one source has been used to implement the 'diversion and sorting' process whereas in the second experiment a source and a sink has been deployed to execute the same.

Diversion using a single source

Manipulation Description:A single source has been used to manipulate two different particles into two different end locations. Both particles have approximately the same initial position within the 'field of view'. With respect to the first particle, source 1 is operated at a strength of 100 ml/hr for the first 47 seconds of its entry, after which it is changed to 250 ml/hr till the particle's exit. As with the second particle, a similar trend is maintained, but the strength is increased from 250 ml/hr to 450ml/hr, after 44 seconds from its entry within the field-of-view. The flow-rate versus time curve of the source used to manipulate above two particles are shown in figures 5.5 and 5.6.

Observation and discussion: The computed and experimental path-lines of the two particles are shown in figures 5.7a and 5.7b. Both particles have an initial x-position of approximately 38 mm. The stream-wise distance for particles to traverse is taken to be 56 mm. A comparison between x and y displacements with respect to time between the experiment and computation for both particles are given in figure5.8 and 5.9. In case of the first particle, the time span in the experiment is found to be approximately 79 seconds, whereas the computed time is approximately 80 seconds as is clear from figure 5.8b. The x-position at the end location is found to be around

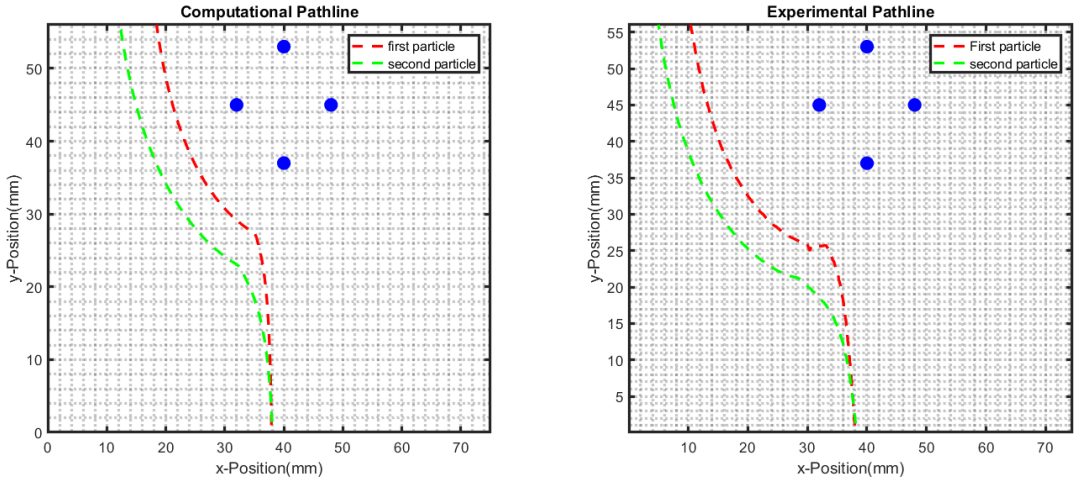

(a) Computational Pathlines (b) Experimental Pathlines

Figure 5.7: Pathlines of the two particles diverted into different outlets.

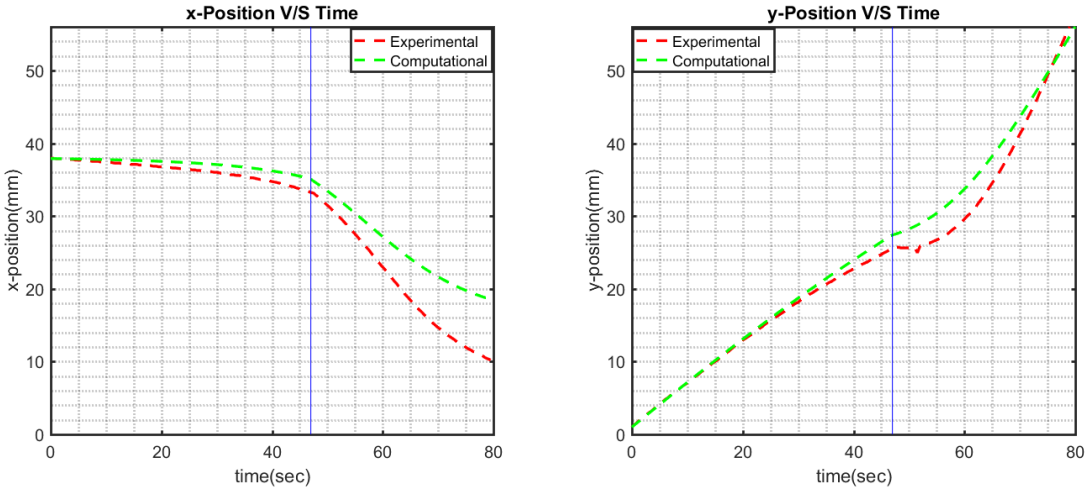

(a) Horizontal displacement of the first particle.The vertical blue line represents the time when the source strength changed from 100 ml/hr to 250 ml/hr.

(b) Vertical displacement of the first particle.The vertical blue line represents the time when the source strength changed from 100 ml/hr to 250 ml/hr.

Figure 5.8: Computational and Experimental Displacement versus Time of the first particle manipulated using a single source.

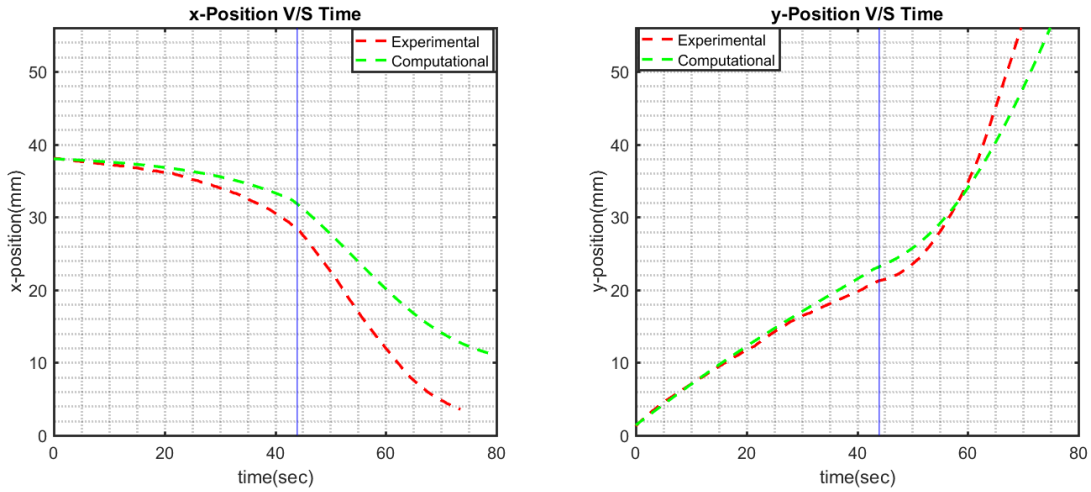

(a) Horizontal displacement of the second particle.The vertical blue line represents the time after which the source strength was changed from 250ml/hr to 450ml/hr.

(b) Vertical displacement of the second particle.The vertical blue line represents the time after which the source strength was changed from 250ml/hr to 450ml/hr.

Figure 5.9: Computational and Experimental Displacement versus Time of the second particle manipulated using a source

10.3 mm, whereas in the computation it is found to be around 18.3 mm(figure5.8a). As with the second particle, the experimental time span in the field-of-view is 69.5 seconds and the corresponding computed value is around 75 seconds(figure5.9b). The x-position at the end of the field-of- view is about 5 mm and 12.5 mm for the experiment and computation respectively(figure5.9a). The deviations in the path-lines of both particles become more pronounced about the vertical blue line, where the steady value of the source changes in the displacement-time curves (figure5.8 and figure5.9). The variations in both the time span and eventual position of the particle can be attributed to the following possible factors : a)The 'skewness effect' which makes the particle biased to a direction; b)The time required for the particle to adjust itself to the new flow field when the flow rate changes; c)The unsteady effect of the flow field itself when the flow rate changes; and d) The finite size of the source which tends to push the streamlines more. These effects are not taken into account while computing. A glimpse on the path-line plots in figure 5.7 also shows that experimental path-lines are wider than computed ones due to the cumulative effect of the above factors.

Diversion using a source and a sink

Manipulation Description: In this experiment, a sink, along with a source has been deployed to guide two separate individual particles into different end locations. The first particle, on its entry, is under the influence of the uniform flow for 25 seconds. After this time, both source-1 and sink-4 are turned on simultaneously, operating at a strength of 150 ml/hr and -150 ml/hr respectively till the particle's exit. For the second particle, which enters the 'field-of-view' from approximately the same initial position, source-1 and sink-4 continues to operate at the above flow rate of 150 ml/hr and -150 ml/hr, but is deactivated after 69 seconds from the particle's entry. The

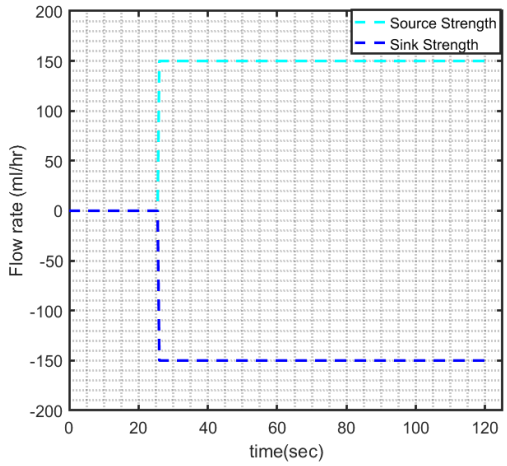

Figure 5.10: Flowrate-time curve of the source and sink used to manipulate the first particle

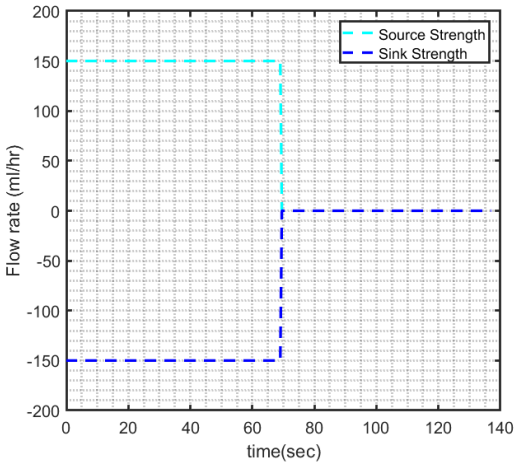

Figure 5.11: Flowrate-time curve of the source and sink used to manipulate the second particle

above unsteady flow field make the particles regain its initial straight trajectories on their exit. The flow-rate time curves are shown in figure 5.10 and 5.11.

Observation and discussion: Figures 5.12a and 5.12b show the computed and experimental path-lines. The displacement-time profiles of both particles are shown in figures 5.13 and 5.14. The total steam-wise length(y-position) is kept at 80 mm. The first particle covers the given distance at approximately 114.5 seconds in the experiment whereas the computed particle time is approximately 117.5 seconds (figure5.13b). The x-position of the first particle at the end of the domain is approximately 28 mm in the experiment, whereas from the computation it is found to be 34.2 mm (figure5.13a). As for the second particle, the time span in the experiment is 129 seconds whereas on computing, the time span is around 134 seconds (figure5.14b). The x-position at the exit is 39.8 mm in the experiment while the computed value is 43.6 mm (figure5.14a). It is to be mentioned that for this particular experiment, although the pinning of the contact angle cannot be completely prevented, the pinning position shifted approximately to the middle of the exit edge of the flow cell, thereby, reducing the skewness angle and hence the biasness. This impact can be observed in figures 5.13a and 5.14a, where the experimental curve remains horizontal and overlaps the computed curve reasonably well over the time particles remain under the influence of the uniform flow, before getting deflected by the dipole. Once the flow field is changed suddenly, slight differences occur between the experiment and computation curves. This is due to the unsteady effect of the particle, when the velocity field is changed and the change in the velocity field itself, in addition to the finite size of the source/sink which are not taken into account while computing.

5.3.2 Trapping and steering

Following the manipulation of particles into different directions, stagnation point in velocity fields have been utilized in order to trap particles and then steering them into different directions.In this section, results of experiments where particles are trapped

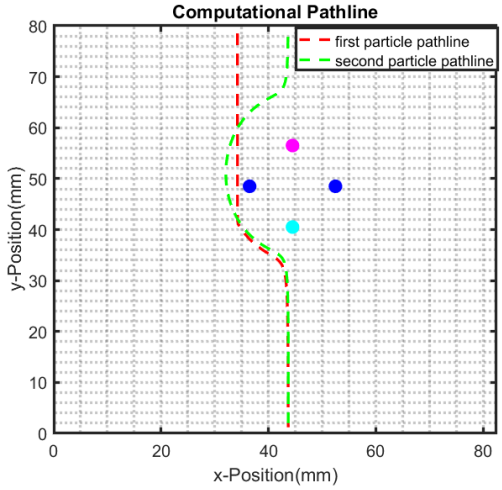

(a) Computational Pathlines

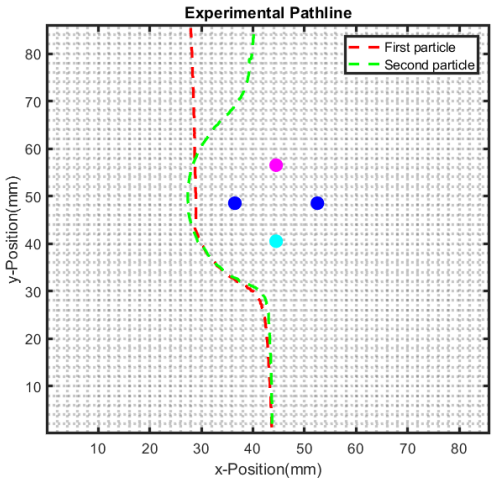

(b) Experimental Pathlines

Figure 5.12: Pathlines of the two particles. The magenta filled circle represents the sink and the cyan filled circle represents the source used to divert the particles.

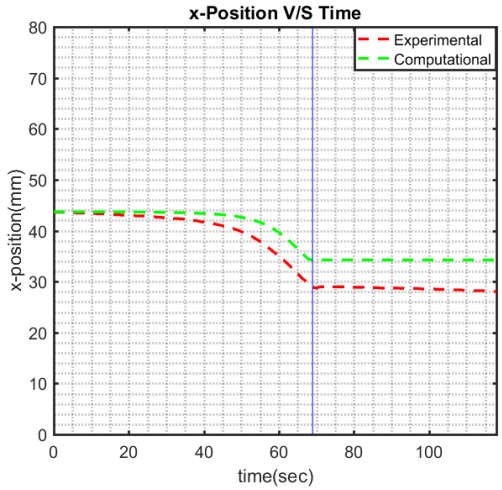

(a) Horizontal displacement of the first particle.The vertical blue line represents the time at which sources and sinks operating at 150ml/hr is deactivated.

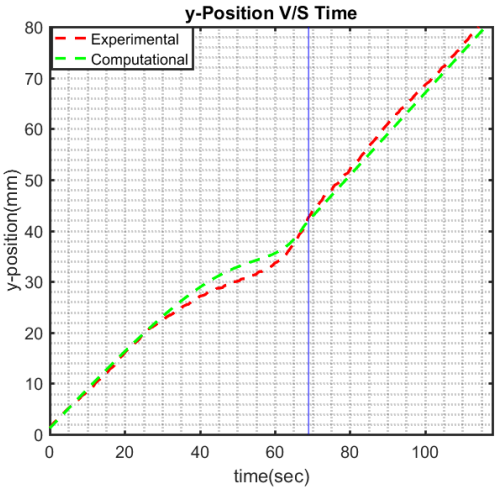

(b) Vertical displacement of the first particle.The vertical blue line represents the time at which sources and sinks operating at 150ml/hr is deactivated.

Figure 5.13: Computational and Experimental Displacement versus Time of the first particle manipulated using a source and a sink.

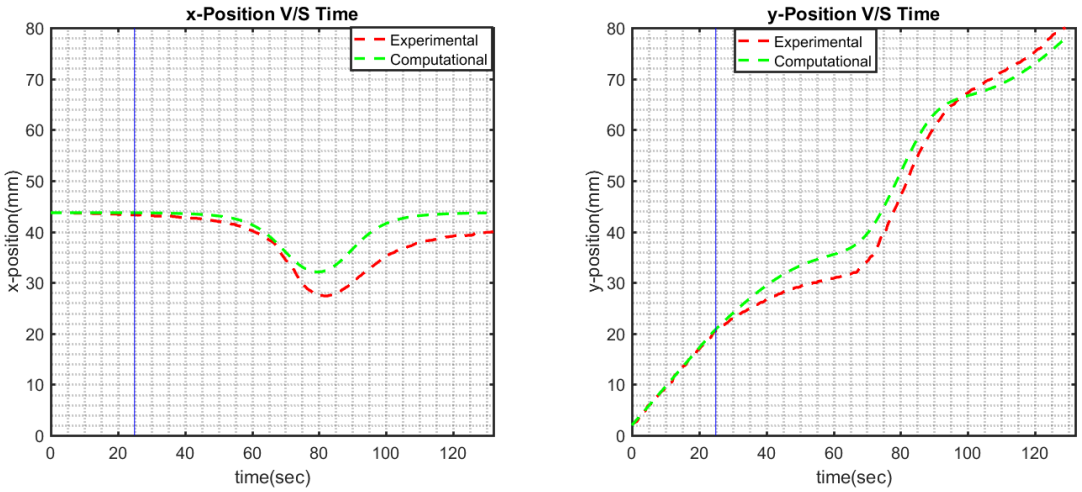

(a) Horizontal displacement of the second particle.The vertical blue line represents the time at which the source and sink of equal strength of 150 ml/hr is activated.

(b) Vertical displacement of the second particle.The vertical blue line represents the time at which the source and sink of equal strength of 150 ml/hr is activated.

Figure 5.14: Computational and Experimental Displacement versus Time of the second particle manipulated using a source and a sink.

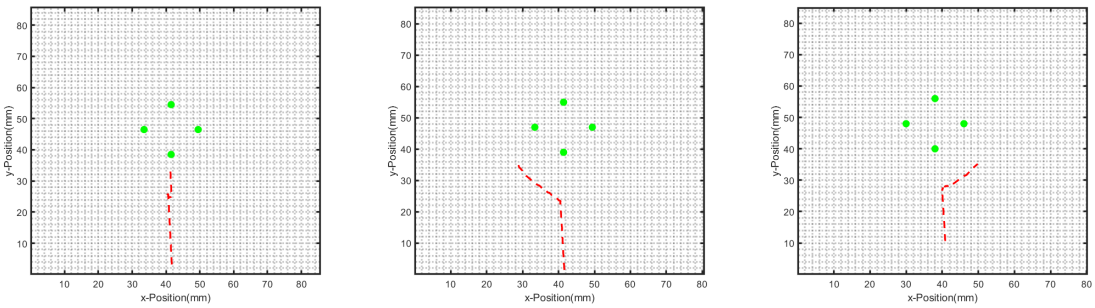

(a) Particle steered straight after being trapped

(b) Particle steered left after being trapped.

(c) Particle steered right after being trapped

Figure 5.15: Pathlines of the trapped particles

and diverted are shown. However, comparison with computations are not performed for the rest of the experiment for reasons explained later in this section. Instead, steady velocity fields used to trap and divert particles are demonstrated. Three experiments exploiting stagnation regions are performed, where a given particle is held for different duration and then subsequently released straight, left and right. The raw images of the above three experiments are given in Appendix A. The path-lines of the three cases are shown in figure 5.15.

As mentioned earlier, computations pertaining to the above three cases have not been performed by the discrete source based Panel method due to fluctuations in the position of the particle around the time it gets trapped. This fluctuation is shown in figure 5.16, which is the magnified image from the path-line figure 5.15a, at the location where the particle is trapped.

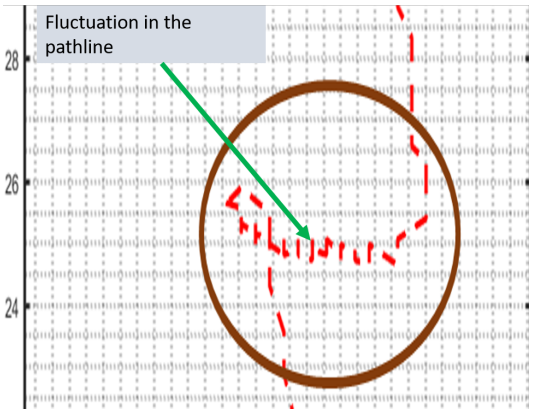

Figure 5.16: Particle fluctuation during the time the particle is being trapped. This is the magnified area around the stagnation region.

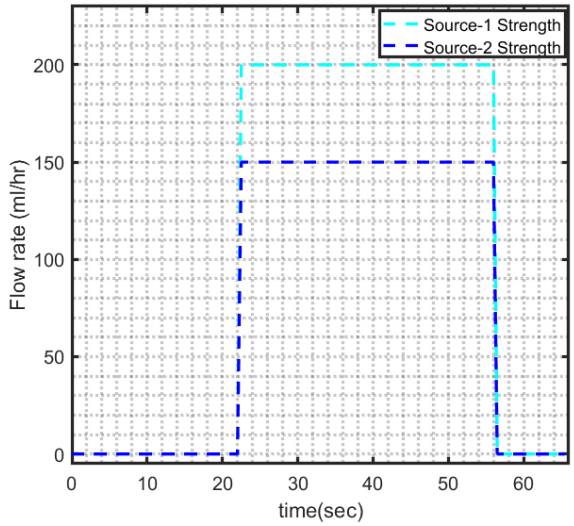

Figure 5.17: Flow-rate time curves of sources used to trap and steer a particle straight.

Trapping and steering straight

For trapping and steering a particle straight, uniform flow is maintained until 22 seconds from the particle's entry. Thereafter, a steady velocity field as shown in figure 5.18 is generated. This is done by activating source 1 to 200 ml/hr and source 2 to 150 ml/hr. Activating these two sources generate a velocity field which has a very low velocity magnitude in the area marked by the rectangular box in figure 5.18. It is important to mention that a single stagnation point is not able to trap a particle because of the fluctuation the particle undergoes, leading to its eventual release. Hence, the idea is to instead create a substantially low velocity field with the use of two sources. Both sources remain active until 56 seconds from the time of the particle's entry into the 'field of view'. Thereafter, uniform flow is maintained to release the particle straight. The time interval between vertical green lines in figure 5.19 is the total time span the particle remains trapped. The flow rate versus time diagram is shown in figure 5.17.

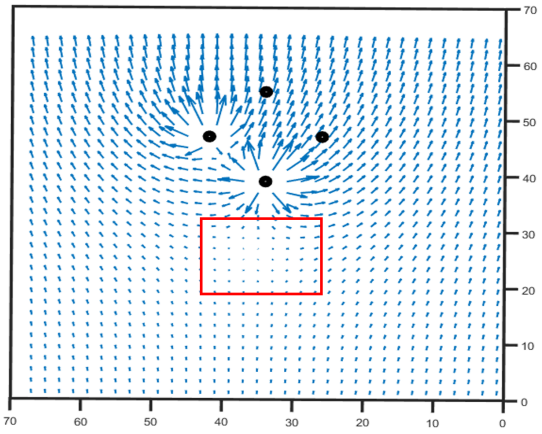

Figure 5.18: Particle is trapped in the area inside the rectangular box where a very low velocity region is created.The direction of the flow is from bottom to top.

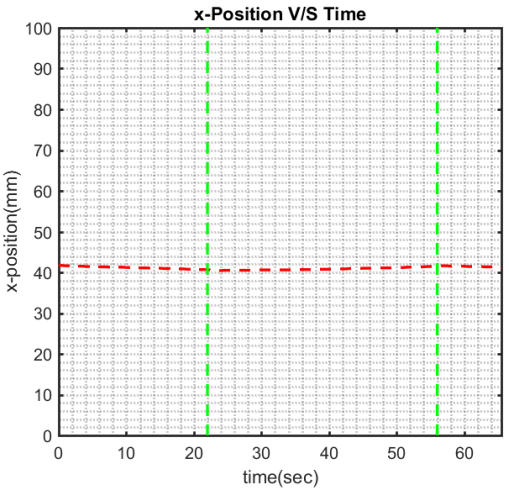

(a) Horizontal displacement of the particle which is trapped and released straight. The region between the vertical green lines show the duration the particle remains stagnant.

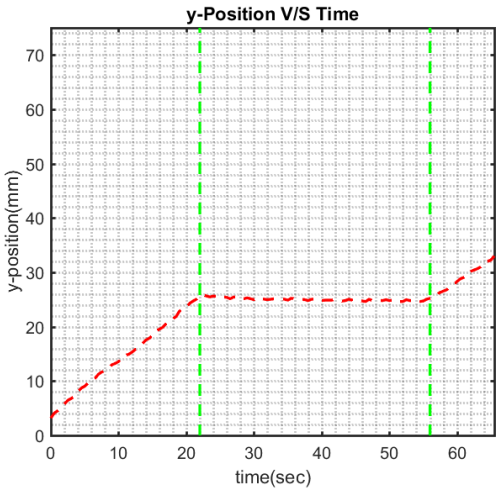

(b) Vertical displacement of the particle which is trapped and released straight. The region between vertical green lines show the duration the particle remains stagnant.

Figure 5.19: Displacement versus time of the particle trapped and steered straight.

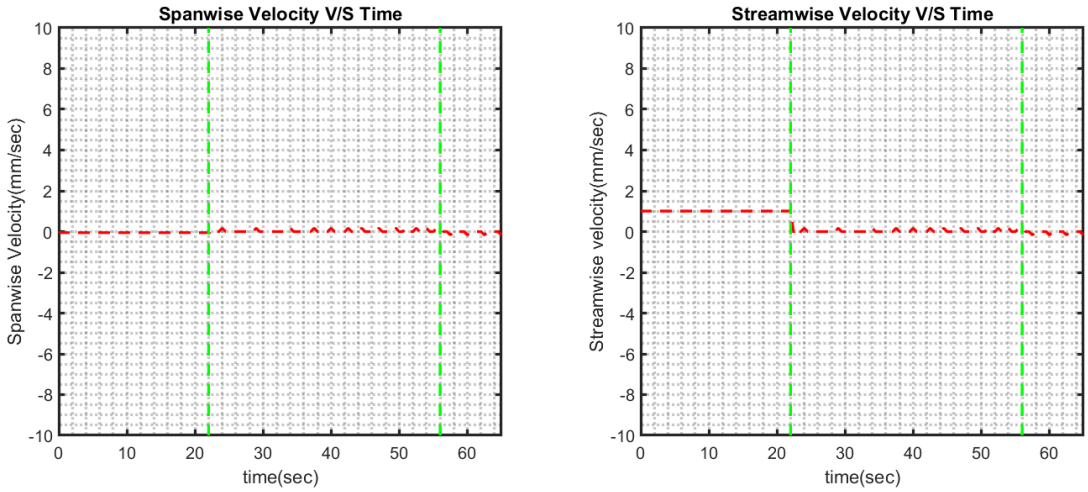

(a) The span-wise velocity of the particle which is trapped and released straight.

(b) The stream-wise velocity of the particle which is trapped and released straight.

Figure 5.20: Velocity versus time of the particle which is trapped and steered straight.

Trapping and steering left

Next, an attempt is made to trap and steer a particle to the left. This is done by generating a field similar to the previous one. After 14 seconds from the particle's entry, source 1 is activated to 250 ml/hr and source 2 to 150 ml/hr. Similar to the previous field, a stagnation region is generated in the area marked by the red rectangular box in figure 5.22, inside which the particle gets trapped. Both sources remain activated from 14 to 23 seconds from the particle's entry, thereby trapping the particle. After 23 seconds, source 2 is changed to a sink operating at -300 ml/hr, with source 1 reduced to 100 ml/hr. The resultant velocity field is shown in figure 5.23, from which it becomes apparent that the particle gets deflected to the left. Combining above two steady fields, individual particle is trapped and steered left. The time interval between vertical green lines in figure 5.24 represents the total time span until which the particle remains stagnant. The flow-rate time curve is shown in figure 5.21.

Trapping and steering right

In order to trap a particle and steer it right, source 1 and 3 are activated to 200 ml/hr and 150 ml/hr respectively. This field is generated after 10.5 seconds from the particle's entry and maintained until 30 seconds, during which the particle remains trapped. Thereafter, source 3 is changed to -200 ml/hr to divert the particle to the right with source 1 reduced to 50 ml/hr. The velocity fields are shown in figure 5.27 and 5.28. The time duration, during which the particle remains stagnant is shown between green vertical lines in figure 5.29.

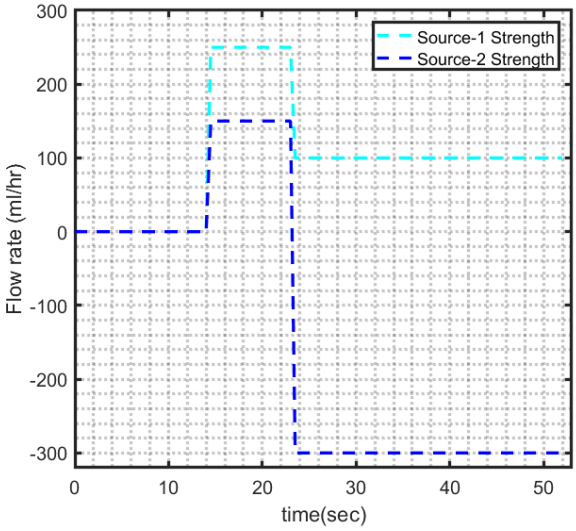

Figure 5.21: Flow-rate time curves of sources used to trap and steer particle left.

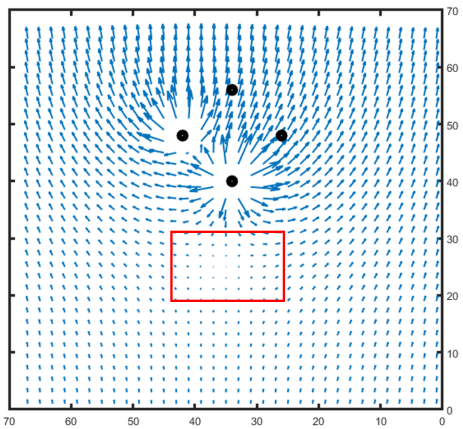

Figure 5.22: Particle is trapped in the area inside the rectangular box where a very low velocity region is created.The direction of the flow is from bottom to top.

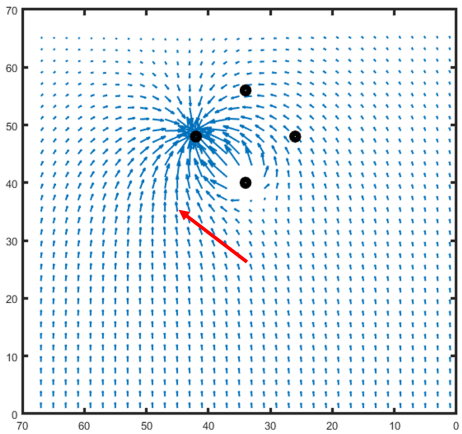

Figure 5.23: The velocity field will deflect the particle to the left.

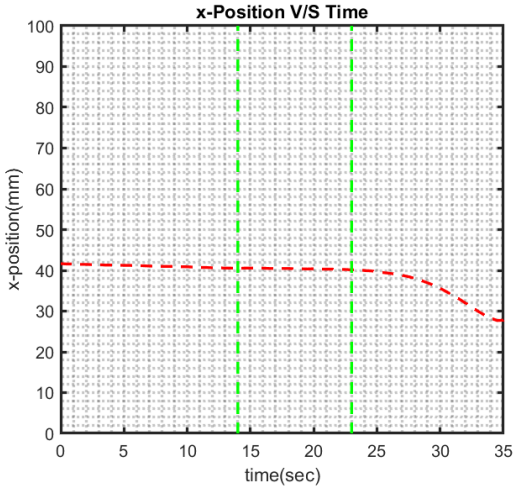

(a) Horizontal displacement of the particle.The region between vertical green lines show the duration the particle remains stagnant.

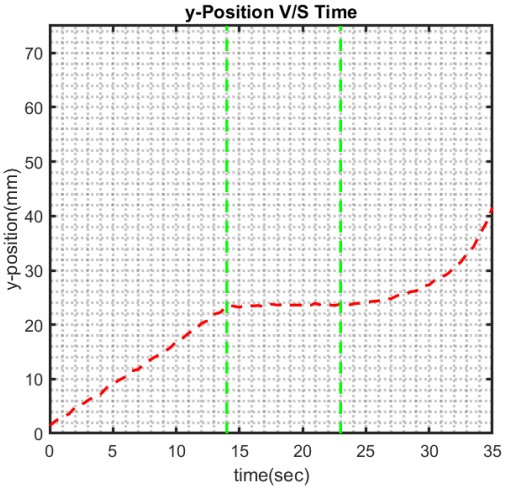

(b) Vertical displacement of the particle. The region between vertical green lines show the time duration which the particle remains stagnant.

Figure 5.24: Displacement versus time of the particle trapped and steered left.

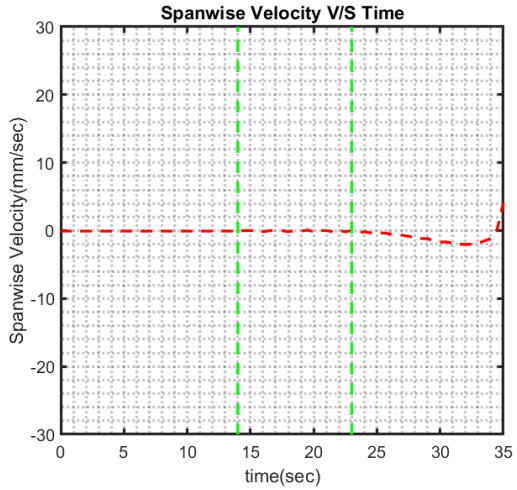

(a) The span-wise velocity of the particle.

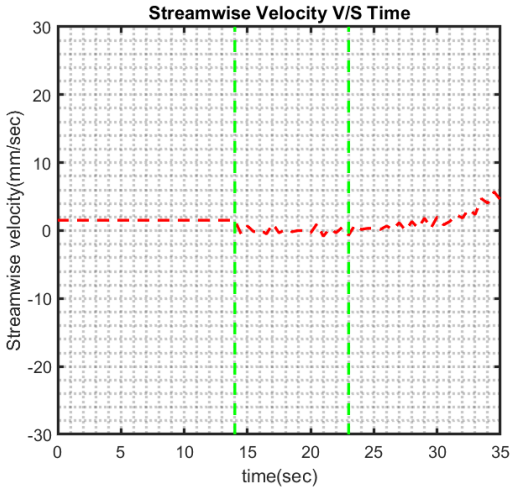

(b) The stream-wise velocity of the particle.

Figure 5.25: Velocity versus time of the particle trapped and steered left.

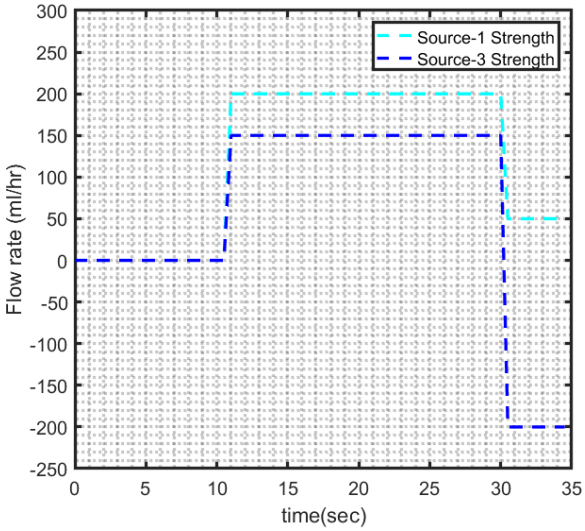

Figure 5.26: Flow-rate time curves of sources used to trap and steer particle right.

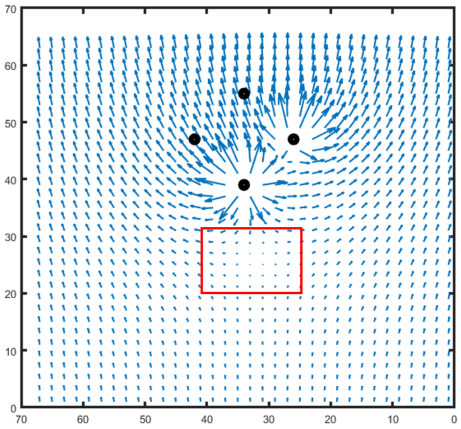

Figure 5.27: Particle trapped inside the area of the rectangular box.

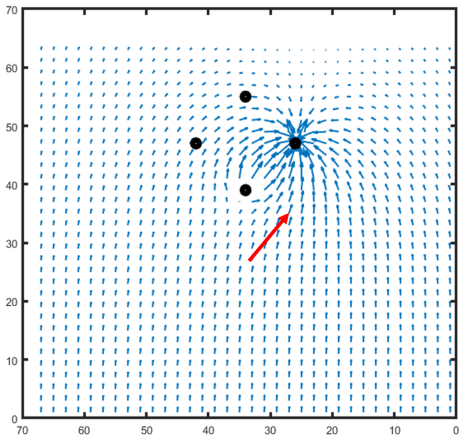

Figure 5.28: The velocity field will deflect the particle to the right.

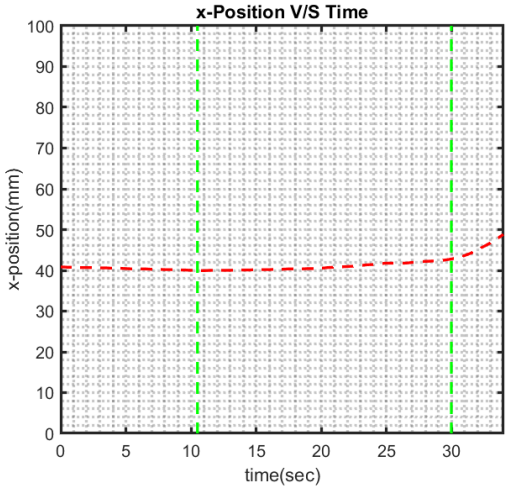

(a) Horizontal displacement of the particle.The region between vertical green lines show the duration the particle remains stagnant.

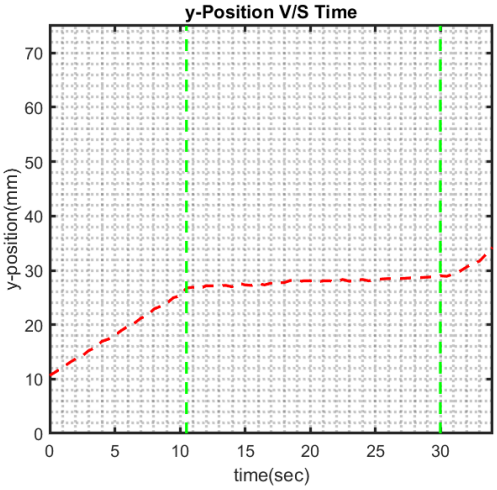

(b) Vertical displacement of the particle.The region between the vertical green lines show the duration the particle remains stagnant.

Figure 5.29: Displacement versus time of the particle trapped and steered right.

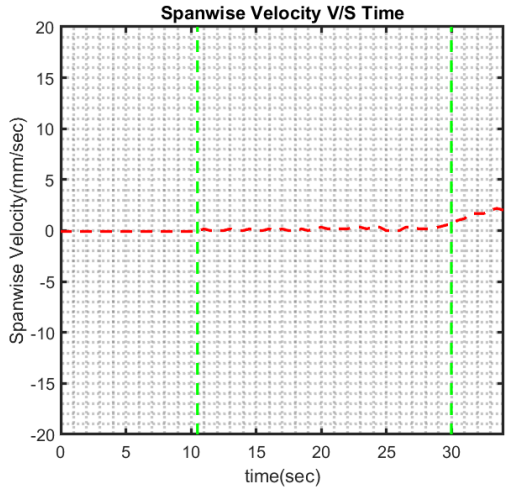

(a) The span-wise velocity of the particle.

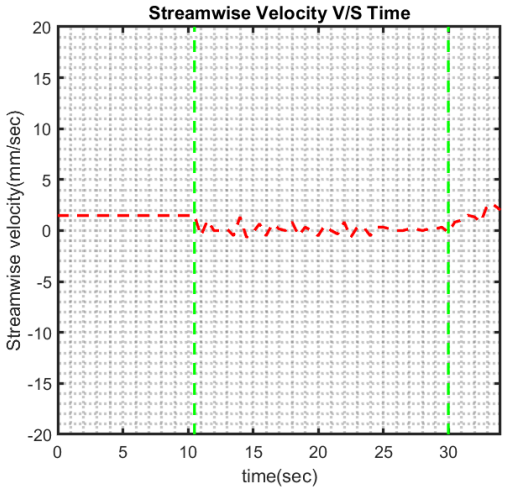

(b) The stream-wise velocity of the particle.

Figure 5.30: Velocity versus time of the particle trapped and steered right.

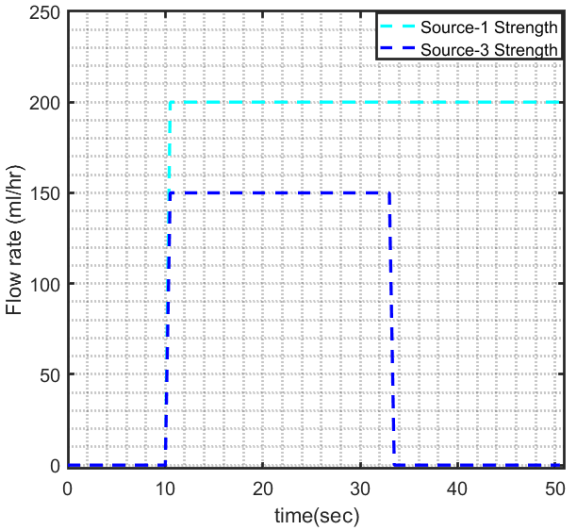

Figure 5.31: Flow-rate time curves of sources used to flip particle position.

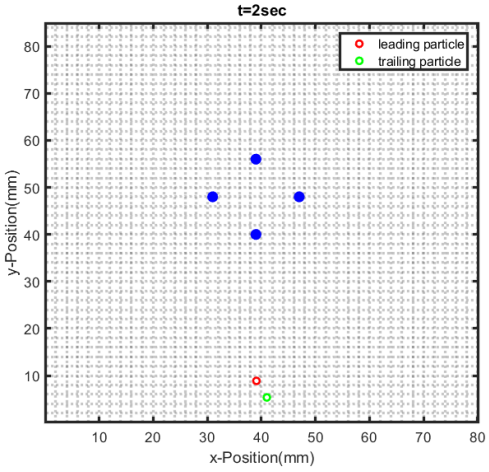

Figure 5.32: Particle positions after 2 seconds.

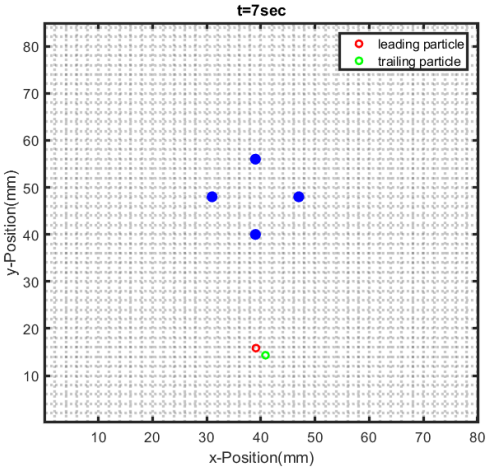

Figure 5.33: Particle positions after 7sec seconds.

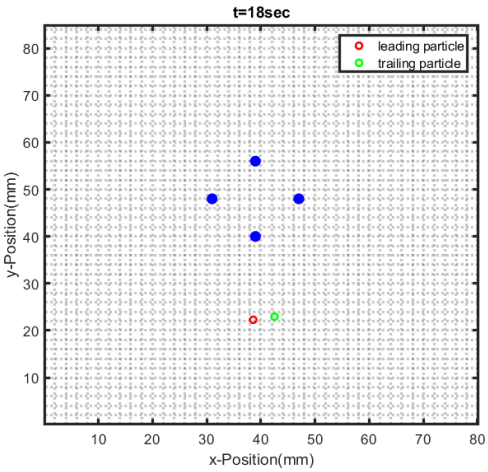

Figure 5.34: Particle positions after 18 seconds.

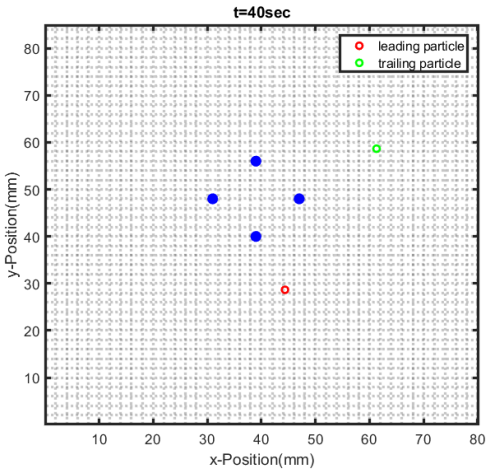

Figure 5.35: Particle positions after 40 seconds.

5.3.3 Flipping particle position

The third manipulation task that is carried out is flipping the position of two particles. The idea of flipping two particles include trapping the 'leading' particle into an area of very low velocity region, until the 'trailing' particle overtakes it. Under the given velocity field, the leading particle follows the streamline which leads directly into the area of very low velocity region. The trailing particle, on the other hand, has an offset with respect to the leading particle in its initial position. As a result, the streamline to which it resorts to deflects it away from the stagnation region, hence, evading its entrapment. The position of two particles at different instances of time, after particle tracking is carried out are shown in figures 5.32, 5.33, 5.34 and 5.35. Particles are initially under the uniform flow for 10 seconds. Thereafter, source 1 and source 3 are activated simultaneously. Source 1 operates at 200 ml/hr whereas source 3 at 150 ml/hr. Velocity fields similar to figure 5.27 is produced, so as to trap the 'leading particle' and allowing the 'trailing particle' to overtake. After approximately 23 seconds from the time of their operation, source 3 is turned off, so that the trapped particle is able to move. The flow rate of the sources in the 'manipulation area' with respect to time is given in figure 5.31. The two velocity fields are shown in figures 5.38 and 5.39. The particle path-line is given in figure 5.37.

5.3.4 Diverting particle by ninety degrees

In order to divert a particle by ninety degrees, source 1 and source 3 are activated simultaneously after 9 seconds from the particle's entry. The strength of source 1 is kept at 250 ml/hr whereas source 2 is used as a sink, operating at -300 ml/hr. 10 seconds from their operation, after the particle has shifted to a position where the influence of sink 2 starts to be more appreciable, sink 2 is switched to a source of strength 300 ml/hr which operates for further 6 seconds before maintaining uniform flow again.

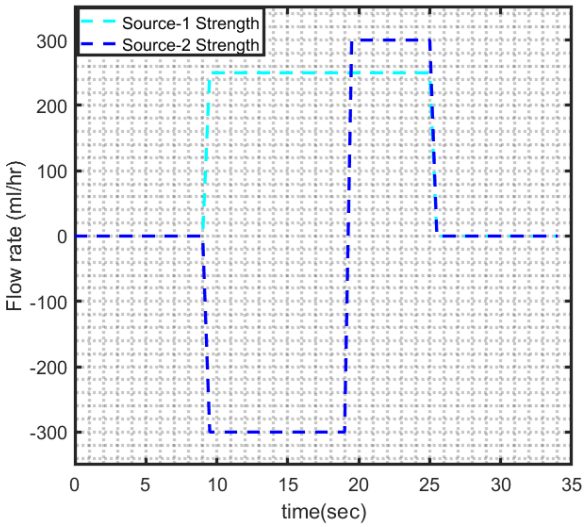

Figure 5.36: Flow-rate time curves of sources used to deflect a particle by ninety degree.

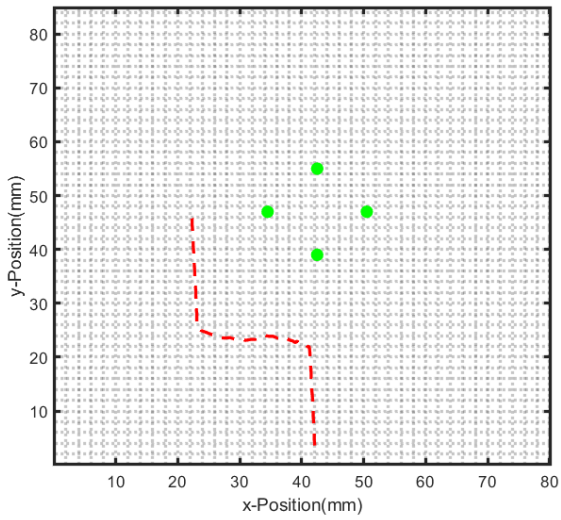

Figure 5.37: Path-line of the particle deflected by ninety degree.

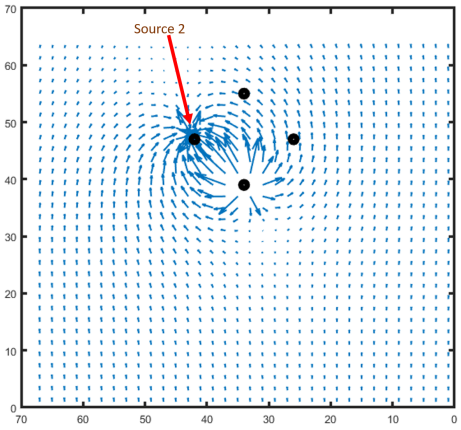

Figure 5.38: Velocity field used from 9 to 19 seconds from the particle's entry where source 2 is used as a sink.

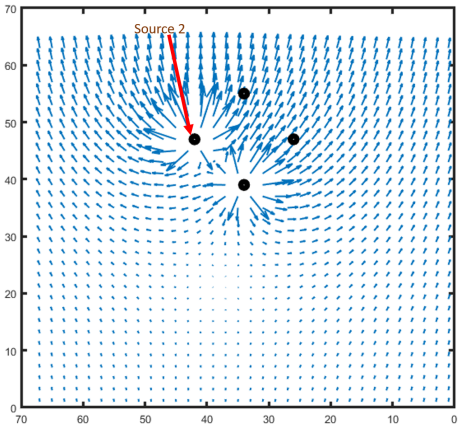

Figure 5.39: Velocity field used from 19 to 25 seconds from the particle's entry where source 2 is switched back to a source.

Chapter 6

Conclusions and Recommendations

This thesis has focused onto the possibility of manipulating particles in a Hele-Shaw cell with the use of sources and sinks. The main contribution of this thesis is towards application in micro-flows, although the work is carried out on a millimeter scale, to check the feasibility of such a technique before reaching the micro-level.

As a first step, a Hele-Shaw cell, suitable for particle manipulation with the aid of source and sinks is designed and constructed. The flow around a Rankine body and the flow around a cylinder are considered for the validation of the design. The maximum half width of the Rankine body and the diameter of the cylinder, as obtained from experiments fall well within the estimated dimensions computed from potential flow theory, thereby, confirming the design validation of the flow cell.

A discrete source based panel method is developed to compute velocity fields that would aid in manipulation of particles. To validate how efficiently the Panel code could replicate streamlines from experiments, volume illuminated PIV measurements of four different steady velocity fields are taken and matched with computation. A good agreement is found between computational streamlines and the experiment. The streamline measurement deviates in the area at location of sources and region having low velocities. This happens due to fluctuations in particle position in and around stagnation regions, causing the particle to move in random direction assisted by constant bombardment of incoming stream of particles. This process leads to yielding spurious vectors. From comparisons between experimental and computational streamlines, it can be inferred that the Panel code can be used to generate streamlines for particle manipulation without delving into PIV measurements.

Finally, individual particles are introduced into the Hele-Shaw flow cell for manipulation. Particles are manipulated using unsteady velocity fields. Based on these velocity fields, individual particles starting from the same initial position have been made to deflect into different end locations. A particle tracking code has been implemented in order to detect individual particle position and generate path lines. These path-lines are then compared to the ones derived from computation using the Panel code and are found to be similar. The difference is found in terms of the total time span and the end position of the vector as the particle exits the field-of-view. The difference may be

attributed to the following possible factors which are not present in the computation: a)The 'skewness effect' due to the pinning of the contact angle at the end; b)unsteady effects of the flow field and the particle when the flow field is changed; c)the finite size of the sources/sinks which pushes streamlines further than expected. Furthermore, ideas stemmed from steady fields generated using The Panel method have been utilized in order to trap individual particles for different duration and subsequently releasing them left, right and straight. Manipulation activities such as flipping the position of two particles and deflecting a particle by ninety degree have also been executed successfully.

6.1 Recommendations for further research

The manipulation of particles(deflections) carried out in this thesis lies in the order of O(10)mm. The deviations between the Panel Method and the experiments are found to be in the order of O(1)mm as far as manipulation with unsteady fields are concerned. Further improvisation on this error can be carried out by working on the three conditions, a)getting rid of the contact-angle pinning at the end of the Hele-Shaw cell. Although measures were taken to get rid of this effect, it cannot be completely prevented. An alternate way to minimize this effect is by increasing the length of the Hele-Shaw, so that the area of interest is far away from the exit where the contact angle pins; b)taking into consideration the unsteady effects of the velocity field and the particle while computing;c)drilling smaller holes for the sources/sinks used to manipulate particles.

Observing the results from particle manipulation, if an error of O(1)mm for deflection seems reasonable for deflection of order O(10) mm, research can be carried out with droplets as well as bubbles, at the scale of the Hele-Shaw cell used for the present thesis.

The current set-up can also be scaled down with the above parameters, as a second step towards reaching to the micro-level. However, for such a case it is recommended to start with particle before using bubble and droplets, as complex flow dynamics are expected for bubbles and droplets.

Bibliography

[1] Ki Wan Bong, Daniel C Pregibon, and Patrick S Doyle. Lock release lithography for 3d and composite microparticles. *Lab on a Chip*, 9(7):863–866, 2009.

[2] Saif A Khan, Axel Günther, Martin A Schmidt, and Klavs F Jensen. Microfluidic synthesis of colloidal silica. *Langmuir*, 20(20):8604–8611, 2004.

[3] Cheng-Chung Lee, Thomas M Snyder, and Stephen R Quake. A microfluidic oligonucleotide synthesizer. *Nucleic acids research*, 38(8):2514–2521, 2010.

[4] Yidan Cui, Feroz M Hameed, Bo Yang, Kyunghee Lee, Catherine Qiurong Pan, Sungsu Park, and Michael Sheetz. Cyclic stretching of soft substrates induces spreading and growth. *Nature communications*, 6, 2015.

[5] Daniel R Gossett, TK Henry, Serena A Lee, Yong Ying, Anne G Lindgren, Otto O Yang, Jianyu Rao, Amander T Clark, and Dino Di Carlo. Hydrodynamic stretching of single cells for large population mechanical phenotyping. *Proceedings of the National Academy of Sciences*, 109(20):7630–7635, 2012.

[6] Jing Dai, Sung Ho Yoon, Hye Young Sim, Yoon Sun Yang, Tae Kwang Oh, Jihyun F Kim, and Jong Wook Hong. Charting microbial phenotypes in multiplex nanoliter batch bioreactors. *Analytical chemistry*, 85(12):5892–5899, 2013.

[7] Matthias Mehling, Tino Frank, Cem Albayrak, and Savaş Tay. Real-time tracking, retrieval and gene expression analysis of migrating human t cells. *Lab on a Chip*, 15(5):1276–1283, 2015.

[8] Alison M Skelley, Oktay Kirak, Heikyung Suh, Rudolf Jaenisch, and Joel Voldman. Microfluidic control of cell pairing and fusion. *Nature methods*, 6(2):147–152, 2009.

[9] Chunhong Zheng, Liang Zhao, Gui'e Chen, Ying Zhou, Yuhong Pang, and Yanyi Huang. Quantitative study of the dynamic tumor–endothelial cell interactions through an integrated microfluidic coculture system. *Analytical chemistry*, 84(4):2088–2093, 2012.

[10] Joost F Swennenhuis, Arjan GJ Tibbe, Michiel Stevens, Madhumohan R Katika, Joost Van Dalum, Hien Duy Tong, Cees JM van Rijn, and Leon WMM Terstappen. Self-seeding microwell chip for the isolation and characterization of single cells. *Lab on a Chip*, 15(14):3039–3046, 2015.

[11] Han Wei Hou, Majid Ebrahimi Warkiani, Bee Luan Khoo, Zi Rui Li, Ross A Soo, Daniel Shao-Weng Tan, Wan-Teck Lim, Jongyoon Han, Ali Asgar S Bhagat, and

Chwee Teck Lim. Isolation and retrieval of circulating tumor cells using centrifugal forces. *Scientific reports*, 3, 2013.

[12] Yoonsun Yang, Hoon Suk Rho, Michiel Stevens, Arjan GJ Tibbe, Han Gardeniers, and Leon WMM Terstappen. Microfluidic device for dna amplification of single cancer cells isolated from whole blood by self-seeding microwells. *Lab on a Chip*, 15(22):4331–4337, 2015.

[13] T Krebs, CPGH Schroen, and RM Boom. A microfluidic study of oil-water separation kinetics. *Advances in Fluid Mechanics IX*, 74:427–438, 2012.

[14] Marc H Schneider, Vincent J Sieben, Abdel M Kharrat, and Farshid Mostowfi. Measurement of asphaltenes using optical spectroscopy on a microfluidic platform. *Analytical chemistry*, 85(10):5153–5160, 2013.

[15] Robert Fisher, Mohammad Khalid Shah, Dmitry Eskin, Kurt Schmidt, Anil Singh, Shahnawaz Molla, and Farshid Mostowfi. Equilibrium gas–oil ratio measurements using a microfluidic technique. *Lab on a Chip*, 13(13):2623–2633, 2013.

[16] Brendon Morin, Yafei Liu, Vladimir Alvarado, and John Oakey. A microfluidic flow focusing platform to screen the evolution of crude oil–brine interfacial elasticity. *Lab on a Chip*, 16(16):3074–3081, 2016.

[17] Douglas Philp and J Fraser Stoddart. Self-assembly in natural and unnatural systems. *Angewandte Chemie International Edition*, 35(11):1154–1196, 1996.

[18] George M Whitesides and Bartosz Grzybowski. Self-assembly at all scales. *Science*, 295(5564):2418–2421, 2002.

[19] Sharon C Glotzer. Some assembly required. *Science*, 306(5695):419–420, 2004.

[20] Kazunori Hoshino, Yu-Yen Huang, Nancy Lane, Michael Huebschman, Jonathan W Uhr, Eugene P Frenkel, and Xiaojing Zhang. Microchip-based immunomagnetic detection of circulating tumor cells. *Lab on a Chip*, 11(20):3449–3457, 2011.

[21] Joo H Kang, Silva Krause, Heather Tobin, Akiko Mammoto, Mathumai Kanapathipillai, and Donald E Ingber. A combined micromagnetic-microfluidic device for rapid capture and culture of rare circulating tumor cells. *Lab on a Chip*, 12(12):2175–2181, 2012.

[22] Xiaoyuan Hu, Paul H Bessette, Jiangrong Qian, Carl D Meinhart, Patrick S Daugherty, and Hyongsok T Soh. Marker-specific sorting of rare cells using dielectrophoresis. *Proceedings of the National Academy of Sciences of the United States of America*, 102(44):15757–15761, 2005.

[23] Eric B Cummings and Anup K Singh. Dielectrophoresis in microchips containing arrays of insulating posts: theoretical and experimental results. *Analytical chemistry*, 75(18):4724–4731, 2003.

[24] Jeffrey R Moffitt, Yann R Chemla, Steven B Smith, and Carlos Bustamante. Recent advances in optical tweezers. *Annual review of biochemistry*, 77, 2008.

[25] A Kasukurti, M Potcoava, SA Desai, C Eggleton, and David WM Marr. Single-cell isolation using a dvd optical pickup. *Optics express*, 19(11):10377–10386, 2011.

[26] Björn Hammarström, Thomas Laurell, and Johan Nilsson. Seed particle-enabled acoustic trapping of bacteria and nanoparticles in continuous flow systems. *Lab on a Chip*, 12(21):4296–4304, 2012.

[27] Andreas Nilsson, Filip Petersson, Henrik Jönsson, and Thomas Laurell. Acoustic control of suspended particles in micro fluidic chips. *Lab on a Chip*, 4(2):131–135, 2004.

[28] Zongbin Liu, Fei Huang, Jinghui Du, Weiliang Shu, Hongtao Feng, Xiaoping Xu, and Yan Chen. Rapid isolation of cancer cells using microfluidic deterministic lateral displacement structure. *Biomicrofluidics*, 7(1):011801, 2013.

[29] Stefan H Holm, Jason P Beech, Michael P Barrett, and Jonas O Tegenfeldt. Separation of parasites from human blood using deterministic lateral displacement. *Lab on a Chip*, 11(7):1326–1332, 2011.

[30] Junya Takagi, Masumi Yamada, Masahiro Yasuda, and Minoru Seki. Continuous particle separation in a microchannel having asymmetrically arranged multiple branches. *Lab on a Chip*, 5(7):778–784, 2005.

[31] Masumi Yamada and Minoru Seki. Microfluidic particle sorter employing flow splitting and recombining. *Analytical chemistry*, 78(4):1357–1362, 2006.

[32] Zhigang Wu, Ben Willing, Joakim Bjerketorp, Janet K Jansson, and Klas Hjort. Soft inertial microfluidics for high throughput separation of bacteria from human blood cells. *Lab on a Chip*, 9(9):1193–1199, 2009.

[33] Dino Di Carlo, Daniel Irimia, Ronald G Tompkins, and Mehmet Toner. Continuous inertial focusing, ordering, and separation of particles in microchannels. *Proceedings of the National Academy of Sciences*, 104(48):18892–18897, 2007.

[34] Soojung Claire Hur, Henry Tat Kwong Tse, and Dino Di Carlo. Sheathless inertial cell ordering for extreme throughput flow cytometry. *Lab on a Chip*, 10(3):274–280, 2010.

[35] DR Link, Shelley L Anna, DA Weitz, and HA Stone. Geometrically mediated breakup of drops in microfluidic devices. *Physical review letters*, 92(5):054503, 2004.

[36] Enkhtuul Surenjav, Craig Priest, Stephan Herminghaus, and Ralf Seemann. Manipulation of gel emulsions by variable microchannel geometry. *Lab on a Chip*, 9(2):325–330, 2009.

[37] Venkatachalam Chokkalingam, Boris Weidenhof, Michael Krämer, Wilhelm F Maier, Stephan Herminghaus, and Ralf Seemann. Optimized droplet-based microfluidics scheme for sol–gel reactions. *Lab on a Chip*, 10(13):1700–1705, 2010.

[38] JM Köhler, Th Henkel, A Grodrian, Th Kirner, M Roth, K Martin, and J Metze. Digital reaction technology by micro segmented flow—components, concepts and applications. *Chemical Engineering Journal*, 101(1):201–216, 2004.

[39] GF Christopher, J Bergstein, NB End, M Poon, C Nguyen, and Shelley L Anna. Coalescence and splitting of confined droplets at microfluidic junctions. *Lab on a Chip*, 9(8):1102–1109, 2009.

[40] Yung-Chieh Tan, Jeffrey S Fisher, Alan I Lee, Vittorio Cristini, and Abraham Phillip Lee. Design of microfluidic channel geometries for the control of droplet volume, chemical concentration, and sorting. *Lab on a Chip*, 4(4):292–298, 2004.

[41] Yung-Chieh Tan, Yao Li Ho, and Abraham Phillip Lee. Droplet coalescence by geometrically mediated flow in microfluidic channels. *Microfluidics and Nanofluidics*, 3(4):495–499, 2007.

[42] AM Leshansky and LM Pismen. Breakup of drops in a microfluidic t junction. *Physics of Fluids*, 21(2):023303, 2009.

[43] Albert Tsung-Hsi Hsieh, Nicole Hori, Rustin Massoudi, Patrick Jen-Hao Pan, Hirotaka Sasaki, Yuh Adam Lin, and Abraham P Lee. Nonviral gene vector formation in monodispersed picolitre incubator for consistent gene delivery. *Lab on a Chip*, 9(18):2638–2643, 2009.

[44] Adam R Abate and David A Weitz. Faster multiple emulsification with drop splitting. *Lab on a Chip*, 11(11):1911–1915, 2011.

[45] Paul Abbyad, Rémi Dangla, Antigoni Alexandrou, and Charles N Baroud. Rails and anchors: guiding and trapping droplet microreactors in two dimensions. *Lab on a Chip*, 11(5):813–821, 2011.

[46] Linas Mazutis and Andrew D Griffiths. Preparation of monodisperse emulsions by hydrodynamic size fractionation. *Applied Physics Letters*, 95(20):204103, 2009.

[47] Thomas Cubaud. Deformation and breakup of high-viscosity droplets with symmetric microfluidic cross flows. *Physical Review E*, 80(2):026307, 2009.

[48] Jean-Christophe Baret, Oliver J Miller, Valerie Taly, Michaël Ryckelynck, Abdeslam El-Harrak, Lucas Frenz, Christian Rick, Michael L Samuels, J Brian Hutchison, Jeremy J Agresti, et al. Fluorescence-activated droplet sorting (fads): efficient microfluidic cell sorting based on enzymatic activity. *Lab on a Chip*, 9(13):1850–1858, 2009.

[49] Luis M Fidalgo, Graeme Whyte, Daniel Bratton, Clemens F Kaminski, Chris Abell, and Wilhelm TS Huck. From microdroplets to microfluidics: selective emulsion separation in microfluidic devices. *Angewandte Chemie International Edition*, 47(11):2042–2045, 2008.

[50] Mitsuhiro Shikida, Kentaro Takayanagi, Kohta Inouchi, Hiroyuki Honda, and Kazuo Sato. Using wettability and interfacial tension to handle droplets of magnetic beads in a micro-chemical-analysis system. *Sensors and Actuators B: Chemical*, 113(1):563–569, 2006.

[51] Kai Zhang, Qionglin Liang, Sai Ma, Xuan Mu, Ping Hu, Yiming Wang, and Guoan Luo. On-chip manipulation of continuous picoliter-volume superparamagnetic droplets using a magnetic force. *Lab on a Chip*, 9(20):2992–2999, 2009.

[52] Charles N Baroud, Jean-Pierre Delville, François Gallaire, and Régis Wunenburger. Thermocapillary valve for droplet production and sorting. *Physical Review E*, 75(4):046302, 2007.

[53] Amar S Basu and Yogesh B Gianchandani. Virtual microfluidic traps, filters, channels and pumps using marangoni flows. *Journal of Micromechanics and Microengineering*, 18(11):115031, 2008.

[54] Neil Reginald Beer, Klint Aaron Rose, and Ian M Kennedy. Monodisperse droplet generation and rapid trapping for single molecule detection and reaction kinetics measurement. *Lab on a Chip*, 9(6):841–844, 2009.

[55] Marc A Unger, Hou-Pu Chou, Todd Thorsen, Axel Scherer, and Stephen R Quake. Monolithic microfabricated valves and pumps by multilayer soft lithography. *Science*, 288(5463):113–116, 2000.

[56] Adam R Abate, Jeremy J Agresti, and David A Weitz. Microfluidic sorting with high-speed single-layer membrane valves. *Applied Physics Letters*, 96(20):203509, 2010.

[57] Otto Manneberg, S Melker Hagsäter, Jessica Svennebring, Hans M Hertz, Jörg P Kutter, Henrik Bruus, and Martin Wiklund. Spatial confinement of ultrasonic force fields in microfluidic channels. *Ultrasonics*, 49(1):112–119, 2009.

[58] Thomas Franke, Adam R Abate, David A Weitz, and Achim Wixforth. Surface acoustic wave (saw) directed droplet flow in microfluidics for pdms devices. *Lab on a Chip*, 9(18):2625–2627, 2009.

[59] Tobias M Schneider, Shreyas Mandre, and Michael P Brenner. Algorithm for a microfluidic assembly line. *Physical review letters*, 106(9):094503, 2011.

[60] Ronald J Adrian and Jerry Westerweel. *Particle image velocimetry*. Number 30. Cambridge University Press, 2011.

Appendix A

Images

A.1 Particle diversion under unsteady field using a source

Raw image of the first particle

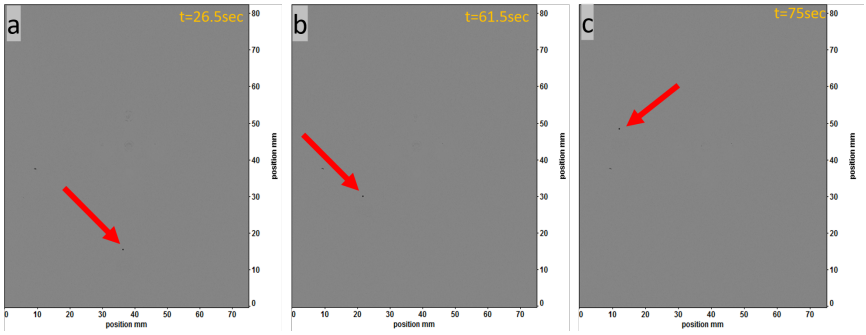

Figure A.1: First Particle positions at different instances of time.

Raw image of the second particle

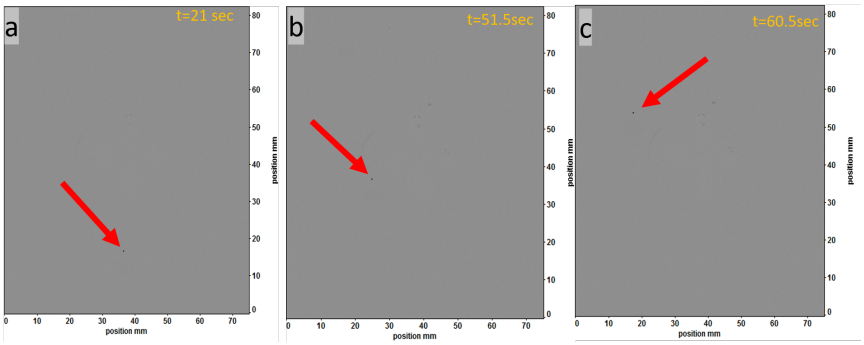

Figure A.2: Second Particle positions at different instances of time.

A.2 Particle diversion under unsteady field using a source and a sink

Raw image of the first particle

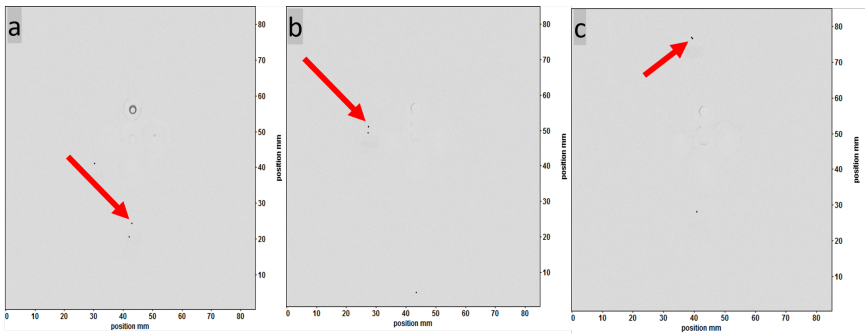

Figure A.3: First Particle positions at different instances of time.

Raw image of the second particle

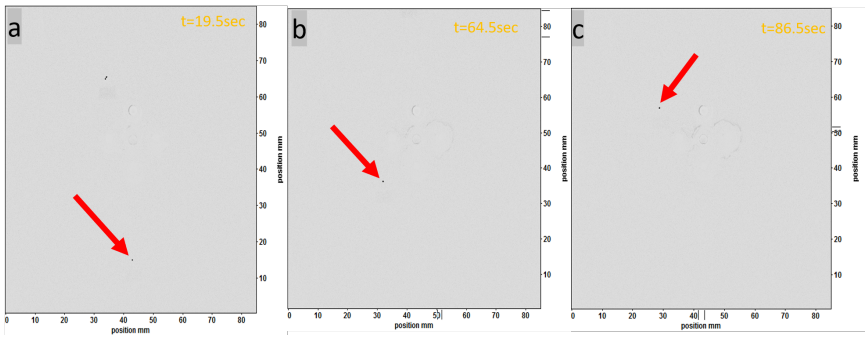

Figure A.4: Second Particle positions at different instances of time.

A.3 Trapping and steering straight

Raw image of the particle being trapped and steered straight.

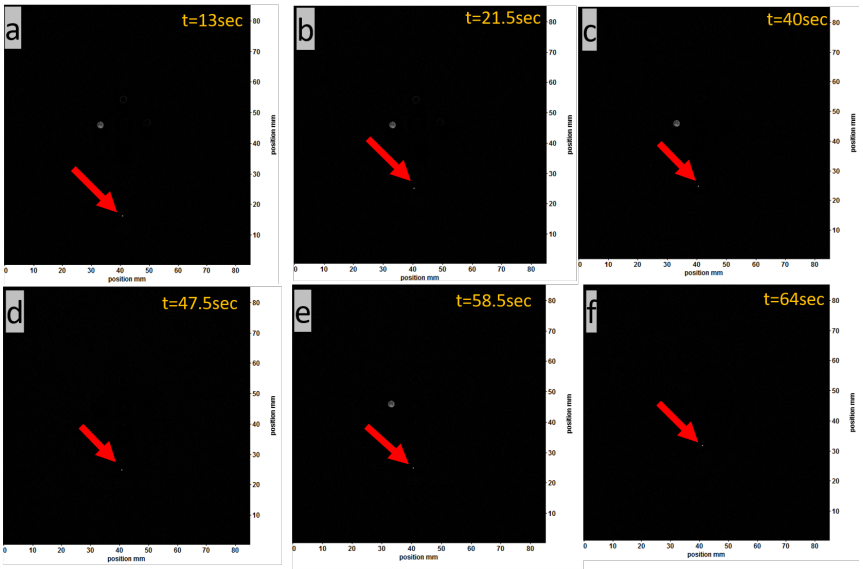

Figure A.5: Images of the particle getting trapped and then being released straight.

A.4 Trapping and steering right

Raw image of the particle being trapped and steered right.

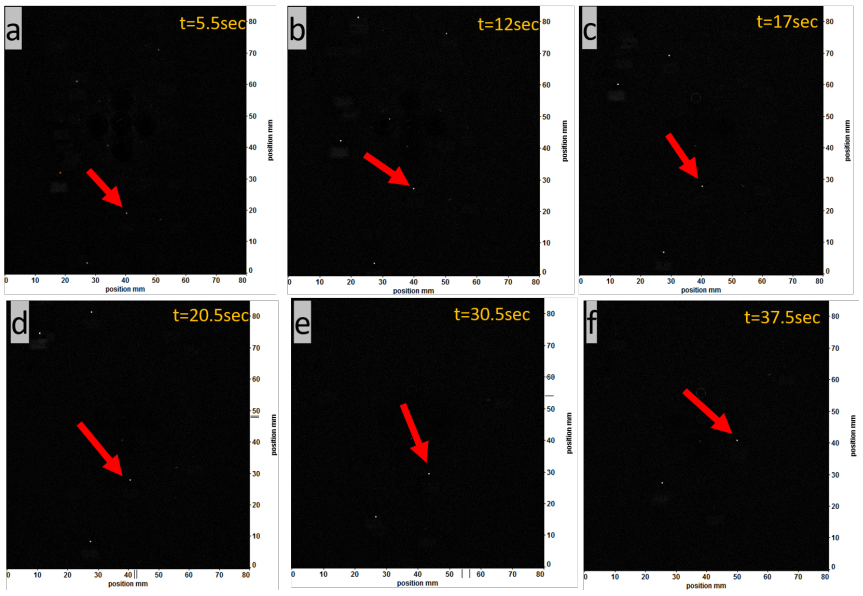

Figure A.6: Images of the particle getting trapped and then being released right.

A.5 Trapping and steering left

Raw image of the particle being trapped and steered left.

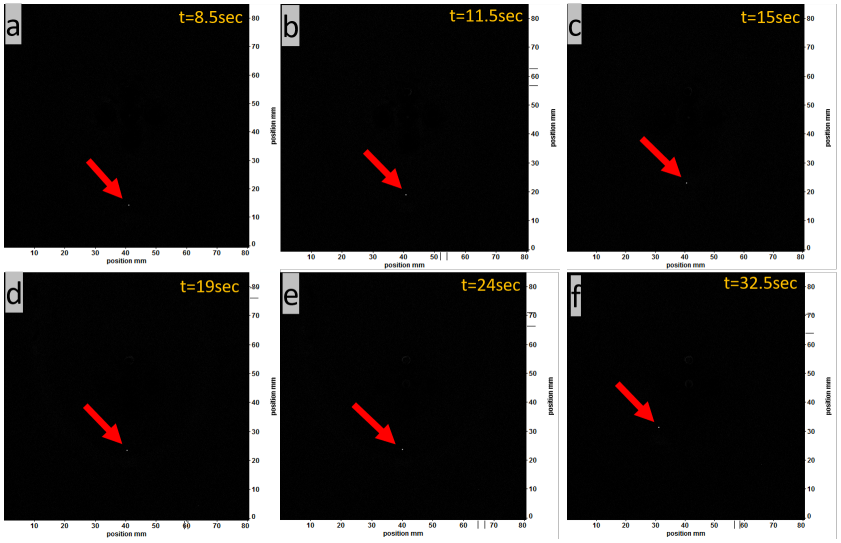

Figure A.7: Images of the particle getting trapped and then being released left.

A.6 flipping particle position

Raw image of the particles being flipped.

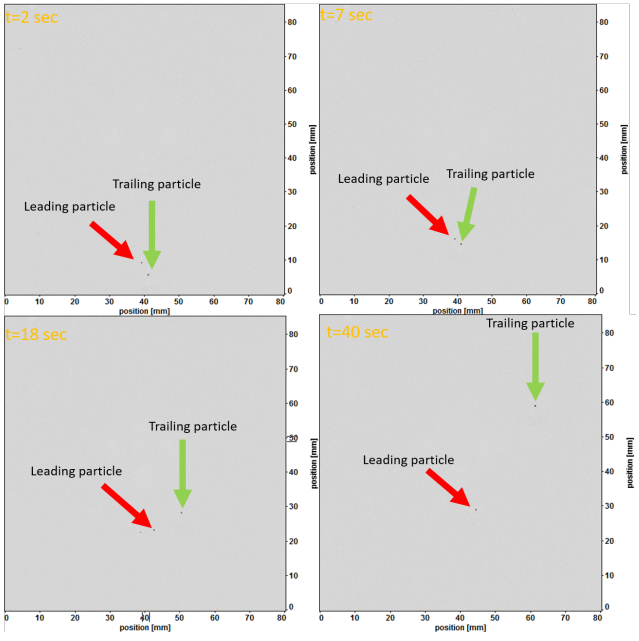

Figure A.8: Images of flipping two particles.

A.7 Diversion of particle by ninety degree

Raw image of the particle being diverted by ninety degree.

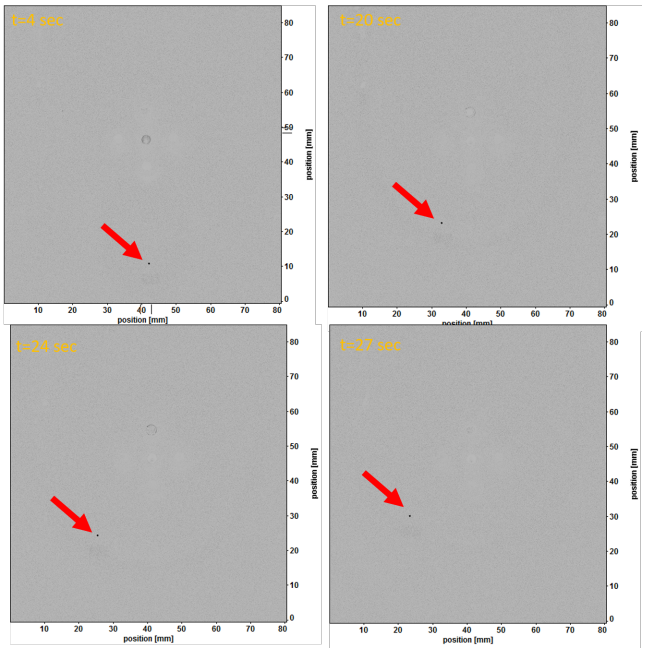

Figure A.9: Images of the particle deflected by ninety degree.

Appendix B

Mass flow rate per unit depth

Choosing mass flow rate per unit depth in the Panel Method

The important parameter while computing is the mass flow rate per unit depth in the Panel Method. In order to choose an appropriate value of the mass flow rate per unit depth in the Panel code, it is necessary to check what velocity the PIV data is measuring. For this data, the PIV results for uniform flow is shown in figure B.1. In this measurement, the uniform flow is driven by three sources of 50ml/hr, 25ml/hr and 50 ml/hr. This gives a total flow rate of 125 ml/hr. The width of the Hele-Shaw cell is 100 mm and the height is 1.5 mm. This should given an average

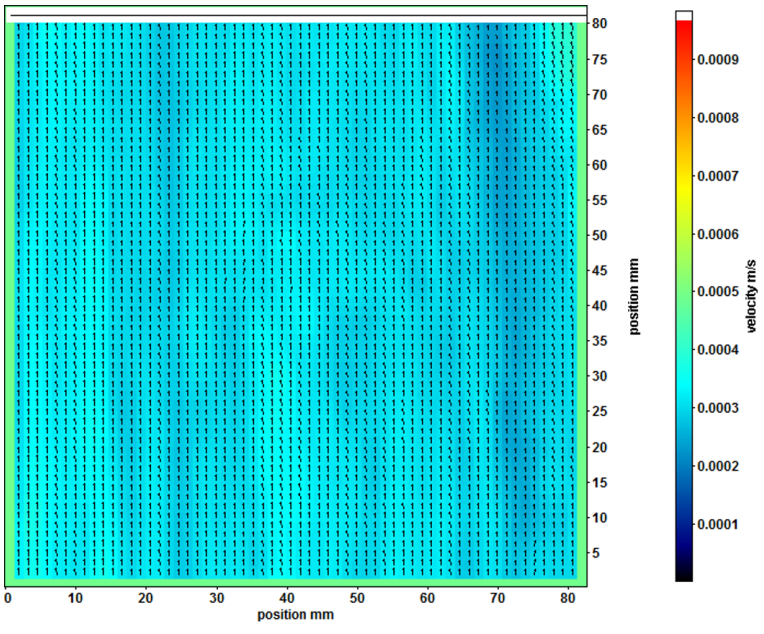

Figure B.1: PIV measurements of the uniform flow

velocity of 0.23 mm/sec. For a Hele- Shaw flow, the maximum center-line velocity is 1.5 times the average velocity, which means the maximum center-line for the above case is approximately, 0.35 mm/sec. However, PIV measurements return a value of approximately 0.3 mm/sec which is 85 percent of the maximum center-line velocity. Coming back to the Panel code, we refer to the mass flow rate per unit depth by $\frac{Q}{h} * k$, where Q is the mass flow rate, h is the height of the Hele-Shaw cell which is

1.5 mm and k is the pre-factor. When k=1, a uniform profile is assumed instead of a parabolic profile and hence, the average flow velocity is returned. The Panel code gives a velocity of 0.21 mm/sec on choosing k=1. Hence, to get a value similar to the PIV measurements which is approximately 0.3 mm/sec, different values of k are tried. On choosing k=1.5, the Panel code returns a value which is approximately equal to the PIV data (0.3 mm/sec). This value of k is chosen in the computation to compare with PIV measurements.

Appendix C

Panel Method

The Panel Method is used to solve flows around arbitrarily shaped bodies in both two and three dimensions. In this method, the body is generally discretized in terms of a singularity distribution of either sources, doublets or vortices. The strengths of these singularities are initially unknown, but are then solved for by enforcing the boundary condition on the body. In the present work, a discrete source based Panel Method is used, in order to take the effect of the side walls, while solving the algebraic Potential flow equation within the flow cell. In order to do this, discrete points called 'source points' are arranged in a U-shaped pattern as shown in figure C.1. However, an offset is maintained from the boundary of the flow cell. The strength of these sources are initially unknown but are to be solved for. In order to do this, group of discrete points called 'collocation points' are introduced on the exact boundary of the flow cell. It is at these points where the 'no penetration' boundary condition is to be satisfied. For the horizontal walls, it is the vertical velocity which has to be zero at the collocation points, whereas for the vertical wall, the horizontal velocity has to be zero. Next step

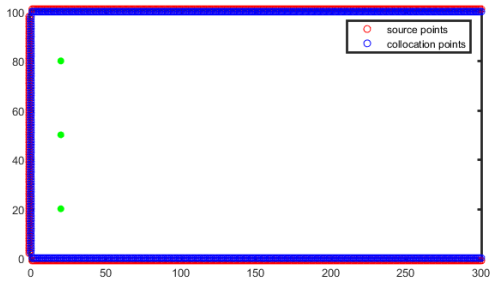

Figure C.1: The computational domain of the flow cell with source and collocation points. The three green filled circles represent upstream sources used to drive the uniform flow. The red circle represents the source points whereas the blue circle represents the collocation points.

is to consider the flow field created by the 'source points' and the actual sources in the domain. Here the case of only three actual sources that drives the uniform flow is considered. In potential flow theory, the flow field due to a single source is given by

$$u = \frac{mx}{2\pi(x^2 + y^2)} \tag{C.1}$$

$$v = \frac{my}{2\pi(x^2 + y^2)} \tag{C.2}$$

where 'm' represents the strength or the flow rate per unit depth. The velocity field of the three actual sources and 'source points' are added to obtain the resultant velocity field, with the strengths of the 'source points' still unknown. To solve for this, the boundary conditions at the 'collocation points' are implemented to obtain a set of linear algebraic equations. Once, this system is solved to obtain the strengths of the 'source points', the final velocity field in the flow cell is computed by superimposing the velocity fields due to the 'source points' and the actual three sources.

Appendix D

Hele-Shaw flow cell equations

Let U be a typical horizontal speed in a domain bounded by $z = 0$ and $z = h(x, y)$. It is assumed that the length scales in the x-y plane have the same order of magnitude given by L, and the variations in the velocity on this plane are of order U. The time scale of the flow is of the order O(L/U). It is also assumed that

$$L >> h \tag{D.1}$$

The effect of gravity is also neglected because of the small height of the channel compared to the other scales. The continuity equation reads as

$$\frac{\partial u}{\partial x} + \frac{\partial v}{\partial y} + \frac{\partial w}{\partial z} = 0 \tag{D.2}$$

The non-dimensional form becomes

$$\frac{U}{L}\frac{\partial \tilde{u}}{\partial \tilde{x}} + \frac{U}{L}\frac{\partial \tilde{v}}{\partial \tilde{y}} + \frac{W}{h}\frac{\partial \tilde{w}}{\partial \tilde{z}} = 0 \tag{D.3}$$

From the non-dimensionalized equation scaling for the w-velocity is obtained as $O(\frac{Uh}{L})$. The x-momentum equation is given by

$$\rho(\frac{\partial u}{\partial t} + u\frac{\partial u}{\partial x} + v\frac{\partial u}{\partial y} + w\frac{\partial u}{\partial z}) = -\frac{\partial p}{\partial x} + \mu(\frac{\partial^2 u}{\partial x^2} + \frac{\partial^2 u}{\partial y^2} + \frac{\partial^2 u}{\partial z^2}) \tag{D.4}$$

On non-dimensionalizing the x-momentum equation we get

$$\frac{\rho U^2}{L}(\frac{\partial \tilde{u}}{\partial \tilde{t}} + \tilde{u}\frac{\partial \tilde{u}}{\partial \tilde{x}} + \tilde{v}\frac{\partial \tilde{u}}{\partial \tilde{y}} + \tilde{w}\frac{\partial \tilde{u}}{\partial \tilde{z}}) = -\frac{\pi}{L}\frac{\partial \tilde{p}}{\partial \tilde{x}} + \mu(\frac{U}{L^2}\frac{\partial^2 \tilde{u}}{\partial \tilde{x}^2} + \frac{U}{L^2}\frac{\partial^2 \tilde{u}}{\partial \tilde{y}^2} + \frac{U}{h^2}\frac{\partial^2 \tilde{u}}{\partial \tilde{z}^2}) \tag{D.5}$$

Applying condition D.1, we get

$$\frac{\rho U^2}{L}(\frac{\partial \tilde{u}}{\partial \tilde{t}} + \tilde{u}\frac{\partial \tilde{u}}{\partial \tilde{x}} + \tilde{v}\frac{\partial \tilde{u}}{\partial \tilde{y}} + \tilde{w}\frac{\partial \tilde{u}}{\partial \tilde{z}}) = -\frac{\pi}{L}\frac{\partial \tilde{p}}{\partial \tilde{x}} + \mu\frac{U}{h^2}\frac{\partial^2 \tilde{u}}{\partial \tilde{z}^2} \tag{D.6}$$

Now if we consider the condition where $(\frac{UL}{\nu})(\frac{h}{L})^2 << 1$, the left side of equation D.6 drops out and the pressure scales with $O(\frac{\mu UL}{h^2})$ The y-momentum will have same

similar characteristic as x-momentum due to similar scaling, hence, the z-momentum equation is considered for further analysis. The z-momentum equation reads as:

$$\rho(\frac{\partial w}{\partial t} + u\frac{\partial w}{\partial x} + v\frac{\partial w}{\partial y} + w\frac{\partial w}{\partial z}) = -\frac{\partial p}{\partial z} + \mu(\frac{\partial^2 w}{\partial x^2} + \frac{\partial^2 w}{\partial y^2} + \frac{\partial^2 w}{\partial z^2}) \tag{D.7}$$

Using the scaling of pressure from the previous equation and scaling of w from the continuity equation, the non-dimensionalized form reads as

$$\frac{\rho U^2 h}{L^2}(\frac{\partial \tilde{w}}{\partial \tilde{t}} + \tilde{w}\frac{\partial \tilde{w}}{\partial \tilde{x}} + \tilde{w}\frac{\partial \tilde{w}}{\partial \tilde{y}} + \tilde{w}\frac{\partial \tilde{w}}{\partial \tilde{z}}) = -\frac{\mu U L}{h^3}\frac{\partial \tilde{p}}{\partial \tilde{z}} + \frac{U\mu h}{L^3}\frac{\partial^2 \tilde{w}}{\partial \tilde{x}^2} + \frac{U\mu h}{L^3}\frac{\partial^2 \tilde{w}}{\partial \tilde{y}^2} + \frac{U\mu}{hL}\frac{\partial^2 \tilde{w}}{\partial \tilde{z}^2} \tag{D.8}$$

Using conditions $L >> h$ and $(\frac{UL}{\nu})(\frac{h}{L})^2 << 1$ shows that the above equation reduces to

$$\frac{\partial \tilde{p}}{\partial \tilde{z}} = 0 \tag{D.9}$$

The final set of equation now reads as

$$\frac{\partial u}{\partial x} + \frac{\partial v}{\partial y} + \frac{\partial w}{\partial z} = 0 \tag{D.10}$$

$$\frac{\partial p}{\partial x} = \mu\frac{\partial^2 u}{\partial z^2} \quad \frac{\partial p}{\partial y} = \mu\frac{\partial^2 u}{\partial z^2} \quad \frac{\partial p}{\partial z} = 0 \tag{D.11}$$

This means that pressure does not vary in the z-direction and x and y momentum equation may be trivially integrated with respect to z. On integrating, the following two equations are obtained from the x and y momentum equations.

$$u = \frac{1}{2\mu}\frac{\partial p}{\partial x}z^2 + Az + B \tag{D.12}$$

$$v = \frac{1}{2\mu}\frac{\partial p}{\partial y}z^2 + +Cz + D \tag{D.13}$$

Applying no-slip boundary conditions at the walls, the constants are solved. In the present thesis work z is bounded by $z = 0$ and $z = h$, hence the solution is of the form

$$u = -\frac{1}{2\mu}\frac{\partial p}{\partial x}z(h - z) \tag{D.14}$$

$$v = -\frac{1}{2\mu}\frac{\partial p}{\partial y}z(h - z) \tag{D.15}$$